Viscosity coefficients for hadron and quark-gluon phases

A.S. Khvorostukhin [a,b], V.D. Toneev [a,c] D.N. Voskresensky [d,c]

[a] *Joint Institute for Nuclear Research, 141980 Dubna, Moscow Region, Russia*

[b] *Institute of Applied Physics, Moldova Academy of Science, MD-2028 Kishineu, Moldova*

[c] *GSI, Plankstraße 1, D-64291 Darmstadt, Germany*

[d] *Moscow Engineering Physical Institute, Kashirskoe Avenue 31, RU-115409 Moscow, Russia*

Abstract

The shear (η) and bulk (ζ) viscosities are calculated in a quasiparticle relaxation time approximation. The hadron phase is described within the relativistic mean field based model with scaled hadron masses and couplings. The quark phase is treated in terms of the heavy quark bag model fitted to the lattice data. A two-phase model allowing for the first order phase transition from the hadron phase to the strongly coupled quark gluon plasma is constructed by means of the Gibbs conditions. Temperature and baryon density dependence of the calculated viscosity-to-entropy ratios (η/s, ζ/s) are analyzed and compared with those obtained in other models. Special attention is paid to the behavior of viscosity coefficients near the critical temperature, from both hadron and quark-gluon side. Effects of resonance widths on viscosities and viscosity-to-entropy ratios are estimated.

1 Introduction

The study of the transport properties of nonequilibrium systems not far from an equilibrium state has a very long story. Methods for the calculation of transport coefficients were probed, e.g., in description of nonrelativistic classical gases [1], liquids and glasses [2], relativistic gases [3], cold atomic gases [4], Fermi [5] and Bose [6] liquids. In the past, transport coefficients for the nuclear matter were also studied [7,8,9,10,11]. A knowledge of various transport coefficients is required also in astrophysical problems such as the entropy production in the universe, the electro-weak baryogenesis [12], for the description

of various phenomena in supernovas and neutron stars [13]. A recent paper [14] considered shear viscosity effects in excited atomic nuclei. With accessibility of heavy-ion collisions the possibility for the creation of a new state of matter, the quark-gluon plasma (QGP), has been offered. In this respect, there appeared growing interest in the calculation of the transport coefficients of the QGP [4,15,16,17,18,19]. Transport coefficients in hot gauge theories were considered in Refs. [20,21,22,23,24,25,26,27]. Attention has mostly been focused on ultrarelativistic theories, where the scale is set exclusively by the temperature T. These results are valid for T much higher than the critical temperature T_c of the deconfinement phase transition. Near the critical temperature the highly nontrivial effects of the strong coupling should be important.

Recently, the interest in the transport coefficient issue has sharply been increased in heavy-ion collision physics. Large values of the elliptic flow v_2 were observed at the Relativistic Heavy Ion Collider [28]. This finding indicates that the created QGP behaves as a nearly perfect fluid with a small value of the shear viscosity-to-entropy density ratio, η/s, which was confirmed by non-ideal hydrodynamic analysis of these data [29]. It was claimed [21,27,30] that a new state produced at high temperatures is most likely not a weakly interacting QGP, as it was originally assumed, but a strongly interacting quark-gluon plasma (sQGP). This interest was also supported by a new theoretical perspective, namely, $\mathcal{N} = 4$ supersymmetric Yang-Mills gauge theory using the Anti de-Sitter space/Conformal Field Theory (AdS/CFT) duality conjecture. Calculations in this strongly coupled theory closely related to QCD give for the η/s ratio [21,25,31]

$$\frac{\eta}{s} = \frac{1}{4\pi}\left(1 + \frac{135\zeta(3)}{8(2\lambda)^{3/2}} + ...\right). \tag{1}$$

This result was confirmed in subsequent investigations [32,33,34]. After evaluating η/s in several strongly coupled theories it was conjectured that $\eta/s = \frac{1}{4\pi}$ is in fact a lower bound on the η/s-ratio in all systems. For certain materials, e.g. helium, nitrogen and water, the η/s-ratio has a minimum at the phase transition [35]. Thus, there appeared belief that QCD nearly saturates mentioned minimum near the critical point of the phase transition [36,37]. These expectations agree with estimates of the shear viscosity obtained within the lattice QCD [38,39,40,41]. Actually, there is an extra contribution of soft modes in the vicinity of the phase transition critical point which may undergo a weak divergence, e.g. for the first order liquid-gas phase transition (H class of universality) one expects the behavior $\eta \propto |T - T_c|^{-\nu/19} \sim |T - T_c|^{-0.034}$, see [42]. However, such a weak divergence can manifest itself only in a very narrow vicinity of the critical point.

The bulk viscosity is much less studied than the shear viscosity. At high tem-

peratures, when coupling is weak and theory is nearly conformal, the bulk viscosity is expected to be very small [17,43,44,45,46]. In liquids the shear and bulk viscosities are usually of the same order of magnitude. However, in some cases the bulk viscosity can be significantly higher than the shear viscosity. This is true in the presence of soft slowly relaxing collective modes. For example, such behavior occurs in the vicinity of the phase transition critical point or at the crossover [46,47,48,49,50,51]. In this case divergence of the bulk viscosity is rather strong, $\zeta \propto |T - T_c|^{-\nu z+\alpha} \sim |T - T_c|^{-1.8}$ (the critical index z is known from the H-model and ν, α from $3d$ Ising model universality class) [42]. Lattice calculations available for the gluon plasma are not in disagreement with the expectation of an increase of the bulk viscosity to the entropy density ratio, ζ/s, toward the QCD phase transition critical point from above but error bars are still very large [40,52]. There are arguments, see [53,54], that the dynamics of the first-order phase transition is controlled by finite values of the kinetic coefficients.

In the modeling of the strongly interacting matter, interactions are often treated within the quasiparticle approximation. Quasiparticle models [55,56] describe the lattice data rather appropriately above the critical temperature T_c. Relativistic mean-field based quasiparticle models were successfully applied to describe the hadron phase [57,58]. In Refs. [45,59] the shear and bulk viscosities of the quark phase were calculated within the quasiparticle approach in the relaxation time approximation in the case where the effective masses of the constituents depend on the temperature and on the baryon density.

In this paper, we extend the investigation of shear and bulk viscosities within the quasiparticle models in the relaxation time approximation [17,45,59]. In Sect. 2, we describe the hadron phase ($T < T_c$) in terms of the quasiparticle relativistic mean-field-based model with the scaling hadron masses and couplings (SHMC) [57,58]. For the QGP phase in Sect. 3 we use the "heavy quark bag" (HQB) model which rather appropriately fits the lattice data. The equation of state for the two-phase SHMC-HQB model is constructed in Sect. 4. In Sects. 5 and 6 we evaluate the shear and bulk viscosities for quasiparticle collisions in the relaxation time approximation and then present results of numerical calculations first for the hadron and then for quark-gluon phases and compare them with previously obtained ones. In Sect. 7, we estimate effects of finite mass-widths of resonances on the viscosities and viscosity-to-entropy ratios. The conclusion remarks are given in Sect. 8. Some details of calculations are deferred to the Appendices A-C.

2 The SHMC model setup

Consider hadronic matter in thermal equilibrium. Within our relativistic mean-field SHMC model we present the Lagrangian density of the hadronic matter as a sum of several terms:

$$\mathcal{L} = \mathcal{L}_{\rm bar} + \mathcal{L}_{\rm MF} + \mathcal{L}_{\rm ex} \ . \tag{2}$$

The Lagrangian density of the baryon component interacting via σ, ω, ρ mean fields is as follows:

$$\mathcal{L}_{\rm bar} = \sum_{b\in\{\rm bar\}} \left[i\bar{\Psi}_b \left(\partial_\mu + i\, g_{\omega b}\, \chi_\omega\ \omega_\mu + i g_{\rho b} \chi_\rho \vec{\rho}_\mu \vec{t}_b \right) \gamma^\mu\, \Psi_b - m_b^*\, \bar{\Psi}_b\, \Psi_b \right] . \tag{3}$$

The considered baryon set is $\{b\} = N(938)$, $\Delta(1232)$, $\Lambda(1116)$, $\Sigma(1193)$, $\Xi(1318)$, $\Sigma^*(1385)$, $\Xi^*(1530)$, and $\Omega(1672)$, including antiparticles. The used σ-field dependent effective masses of baryons are [57,58,60]

$$m_b^*/m_b = \Phi_b(\chi_\sigma \sigma) = 1 - g_{\sigma b}\ \chi_\sigma\ \sigma/m_b\,,\ b \in \{b\}\ . \tag{4}$$

In Eqs. (3), (4) $g_{\sigma b}$, $g_{\omega b}$, $g_{\rho b}$ are coupling constants and $\chi_\sigma(\sigma)$, $\chi_\omega(\sigma)$, $\chi_\rho(\sigma)$ are coupling scaling functions.

The σ-, ω-, ρ-meson contribution is

$$\begin{aligned} \mathcal{L}_{\rm MF} =& \frac{\partial^\mu\sigma\ \partial_\mu\sigma}{2} - \frac{m_\sigma^{*2}\,\sigma^2}{2} - U(\sigma) - \frac{\omega_{\mu\nu}\,\omega^{\mu\nu}}{4} + \frac{m_\omega^{*2}\,\omega_\mu\omega^\mu}{2} \\ & - \frac{\vec{\rho}_{\mu\nu}\,\vec{\rho}^{\mu\nu}}{4} + \frac{m_\rho^{*2}\,\vec{\rho}_\mu\vec{\rho}^\mu}{2}, \\ \omega_{\mu\nu} =& \partial_\mu\omega_\nu - \partial_\nu\omega_\mu\ \ , \quad \vec{\rho}_{\mu\nu} = \partial_\mu\vec{\rho}_\nu - \partial_\nu\vec{\rho}_\mu\ . \end{aligned} \tag{5}$$

The mass terms of the mean fields are

$$m_m^*/m_m = |\Phi_m(\chi_\sigma\sigma)|\,, \quad \{m\} = \sigma, \omega, \rho\,. \tag{6}$$

The dimensionless scaling functions Φ_b and Φ_m, as well as the coupling scaling functions χ_m depend on the scalar field in the combination $\chi_\sigma(\sigma)\ \sigma$. Following [60] we assume approximate validity of the Brown-Rho scaling ansatz in the simplest form

$$\Phi = \Phi_N = \Phi_\sigma = \Phi_\omega = \Phi_\rho = 1 - f, \quad f = g_{\sigma N}\ \chi_\sigma\ \sigma/m_N \tag{7}$$

with $\chi_\sigma = \Phi_\sigma$.

We keep a standard form for the potential of the non-linear self-interaction U used in relativistic mean-field models, now expressed in terms of f-variable:

$$U = m_N^4 (\frac{b}{3}\, f^3 + \frac{c}{4}\, f^4). \tag{8}$$

The third term in the Lagrangian density (2) includes meson excitations

$$\mathcal{L}_{\rm ex} = \sum_{\rm bos\in\{ex\}} \mathcal{L}_{\rm bos}, \tag{9}$$
$$\{\rm ex\} = \pi; K, \bar{K}; \eta(547); \sigma', \omega', \rho'; K^*, \bar{K}^*(892), \eta'(958), \phi(1020).$$

The knowledge of the Lagrangian density (2) defines unambiguously the energy-momentum tensor $T_{\mu\nu}$ (Greek indices μ, ν run $0, 1, 2, 3$). The energy density E and pressure P are given by the diagonal terms of the energy-momentum tensor $E = \langle T_{00} \rangle\,,\ P = \frac{1}{3} \langle T_{ii} \rangle$, Latin index $i = 1, 2, 3$. The pressure can be presented as a sum of the mean-field terms and contributions of the baryons and meson excitations [57,58]:

$$P[f, \omega_0] = P_{\rm MF}[f, \omega_0] + \sum_{b\in\{\rm bar\}} P_b[f, \omega_0] + \sum_{\rm bos\in\{ex\}} P_{\rm bos}[f, \omega_0]\ . \tag{10}$$

Below we consider isospin-symmetric nuclear matter ($N = Z$). Then there are only σ and ω_0 mean field solutions of equations of motion. Therefore further we set the mean fields $\vec{\omega} = 0$ and $\vec{\rho}_\mu = 0$. The value of the mean field $\omega_0(f)$ is found by minimization of the pressure and then it is plugged back in the pressure functional. The latter becomes a function only of f. The equilibrium value of f can be found by subsequent minimization of the resulting pressure in this field. In a self-consistent treatment [58], equations of motion for the mean fields render

$$\frac{\partial}{\partial \omega_0} P[f, \omega_0] = 0\ , \quad \frac{d}{df} P[f, \omega_0(f)] = \frac{\partial}{\partial f} P[f, \omega_0(f)] = 0\ . \tag{11}$$

Since the boson excitation term depends on the mean fields, its minimization produces extra terms in the equations of motion for the mean fields. This self-consistency of the scheme allows us to be sure of thermodynamic consistency of the model.

It is convenient to introduce renormalized constants

$$C_m = \frac{m_N \; g_{mN}}{m_m} \tag{12}$$

and, instead of χ_m, consider other functions

$$\eta_m(f) = \Phi_m^2(f)/\chi_m^2(f) \;\; \text{for } \{m\} = \omega, \rho \; , \quad \eta_\sigma(f) = 1. \tag{13}$$

In terms of this new notation the contribution of mean fields to the pressure (10) is :

$$P_{\rm MF}[f, \omega_0] = -\frac{m_N^4 \, f^2}{2\, C_\sigma^2}\, \eta_\sigma(f) - U(f) + \frac{m_N^2 \eta_\omega(f)}{2\, C_\omega^2}\, \left[g_{\omega N}\, \chi_\omega\, \omega_0\right]^2 . \tag{14}$$

The density of particle species a is given by

$$n_a(T, \mu_a) = \frac{\nu_a}{2\pi^2} \int_0^\infty d|\vec{p}| \;\; |\vec{p}|^2 \;\; F_a^{\rm eq}(k, T, \mu_a) \; . \tag{15}$$

The corresponding contribution to the pressure in (10) is as follows:

$$P_a[f, \omega_0] = \frac{\nu_a}{3} \int\limits_0^\infty \frac{{\rm d}|\vec{p}_a| \;\; |\vec{p}_a|^4}{2\pi^2} \, \frac{F_a^{\rm eq}}{E_a} \; . \tag{16}$$

Here $a = (b \in \{\rm bar\}, {\rm bos} \in \{\rm ex\})$, "$b$" is the baryon and antibaryon, "bos" is the boson and antiboson excitation as described above; ν_a is the degeneracy factor;

$$F_a^{\rm eq} = \left[e^{(E_a - \mu_a^*)/T} \pm 1\right]^{-1} \tag{17}$$

is the quasiparticle occupation for fermions (+) and bosons (−) with the quasiparticle energy

$$E_a = \sqrt{(m_a^{\rm part*})^2 + \vec{p}_a^{\,2}} \; , \tag{18}$$

effective mass $m_a^{\rm part*}$ and the gauge-shifted values of chemical potentials

$$\mu_b^* = t_b^{\rm bar}\mu_{\rm bar} + t_b^{\rm str}\ \mu_{\rm str} - t_b^{\rm vec}\ g_{\omega b}\ \chi_\omega\ \omega_0 = \mu_b - t_b^{\rm vec}\ g_{\omega b}^*\omega_0,$$
$$\mu_{\rm bos}^* = t_{\rm bos}^{\rm str}\ \mu_{\rm str} - t_{\rm bos}^{\rm vec}\ g_{\omega,{\rm bos}}^*\ \omega_0 = \mu_{\rm bos} - t_{\rm bos}^{\rm vec}\ g_{\omega,{\rm bos}}^*\ \omega_0. \qquad (19)$$

Baryon (antibaryon) quantum numbers $t_b^{\rm bar}$, $t_b^{\rm str}$, $t_b^{\rm vec}$ are the baryon charge, strangeness and vector charge, $t_{\rm bos}^{\rm vec}$ is the vector charge of the boson (antiboson) excitation; $g_{\omega,{\rm bos}}^*$ are effective coupling constants. We use the same values of the effective coupling constants and masses as in [58]. One should specially note that as in Ref. [58] here and below the coupling constants $g_{\sigma b}$, except for nucleons, are additionally suppressed by factor 1/10 compared to values which are usually used, see Fig. 3 in [58]. This allows us to fit the lattice results for the pressure of the quark phase up to $T \sim (220 \div 230)$ MeV with our SHMC model.

Summing up over all relevant hadron species we obtain the total baryon charge and strangeness in the hadron phase

$$n_{bar}(T,\mu_{\rm bar},\mu_{\rm str}) = \sum_{a\in\{h\}} b_a\ n_a(T,\mu_a)\ , \qquad (20)$$
$$n_{\rm str}(T,\mu_{\rm bar},\mu_{\rm str}) = \sum_{a\in\{h\}} s_a\ n_a(T,\mu_a), \qquad (21)$$

where the sum is taken over all hadrons $\{h\} = \{b\} + \{{\rm bos}\}$.

The pressure of boson excitations [1] is the pressure of the ideal Bose-gas of quasiparticles in the mean fields with effective masses for σ-, ω-, ρ- field excitations and K mesons, see (16) – (19). For other particles we use bare masses.

In order to get $P_\sigma^{\rm part}$, we should expand total pressure $P[\sigma,\omega_0(\sigma)]$ in $\sigma^{'} = \sigma - \sigma^{\rm cl}$. The term linear in $\sigma^{'}$ does not contribute due to the subsequent requirement of the pressure minimum in $\sigma^{\rm cl}$, $dP/df = 0$. The quadratic term produces effective $\sigma^{'}$- particle mass squared,

$$(m_\sigma^{\rm part*})^2 = -\frac{d^2P_{\rm MF}[\sigma,\omega_0(\sigma)]}{d\sigma^2} = -\frac{d^2P_{\rm MF}[f,\omega_0(f)]}{df^2}\left(\frac{df}{d\sigma}\right)^2. \qquad (22)$$

Keeping only quadratic terms in all thermodynamical quantities in fluctuating fields we disregard the boson excitation and the baryon contributions in (22). Within our approximation the effective masses of ω- and ρ- excitations prove to be the same as those following from the mean-field mass terms

[1] We pay attention to a misprint in Eq. (33) of [58] for the kaon contribution. In denominator enter $\omega_K[\omega_0 = R_0 = 0]$.

$$m_\omega^{\rm part*} = m_\omega |\Phi_\omega(f)|, \quad m_\rho^{\rm part*} = m_\rho |\Phi_\omega(f)| \ . \tag{23}$$

We compare the results of our SHMC model with those for the ideal gas (IG) of free particles. In the IG approximation the density of the particle of the species a with the spin-isospin degeneracy factor ν_a is

$$n_a^{\rm IG}(T,\mu_a) = \frac{\nu_a}{2\pi^2}\int_0^\infty dk\ k^2\ F_a^{\rm IG}(k,T,\mu_a)\ , \tag{24}$$

where

$$F_a^{\rm IG}(k,T,\mu_a) = \left[\ \exp\left(\frac{\sqrt{k^2+m_a^2}-\mu_a}{T}\right) \pm 1\right]^{-1} \tag{25}$$

is the momentum distribution for fermions (upper sign +) and bosons (lower sign −) in the IG limit. Here the chemical potential

$$\mu_a = b_a\ \mu_{\rm bar} + s_a\ \mu_{\rm str} \tag{26}$$

is related to the baryon $\mu_{\rm bar}$ and strange $\mu_{\rm str}$ chemical potentials which control the conservation of the baryon and strangeness charges, respectively; b_a, s_a are the baryon/antibaryon charge and strangeness for the given species.

In Fig. 1 (left panel) we show the square of the speed of sound $c_s^2 = dP/d\varepsilon$ at $\mu_{\rm bar} = 0$ for the SHMC model (solid line) and compare the result with that for the IG model with different species number: with the same hadron set as in the SHMC model (long-dashed line), for a $\pi+\rho$ mixture (dash-double-dotted) and for a purely pion system (dash-dotted). Short-dashed line shows c_s^2 for the Hagedorn model (*i.e.* an IG of hadron resonances whose mass spectrum is assumed to have the Hagedorn form $\rho(m) = m^{-a}\ \exp(m/T_{\rm H})$ where $a = 4$ and T_H is interpreted as an upper bound of the hadron temperature [61,62]).

As is seen, for the pure pion IG the c_s^2 monotonously increases with increase of the temperature approaching the ultrarelativistic limit $c_s^2 = 1/3$ at high temperatures. For the pion-rho meson mixture, the c_s^2 exhibits a shallow minimum at $T \sim 170$ MeV. The minimum (in the same temperature region) is getting more pronounced for multi-component systems (see long-dashed curve). At $T \lesssim 50$ MeV the pion contribution is a dominant one, thereby all curves coincide [2]. The curves for the SHMC model and IG calculated with the same hadron set coincide for $T \lesssim 100$ MeV. At $T > 50$ MeV heavier mesons start to contribute that slows down the growth of the pressure and then results in

[2] Note that within the SHMC model pions are treated as an ideal particle gas

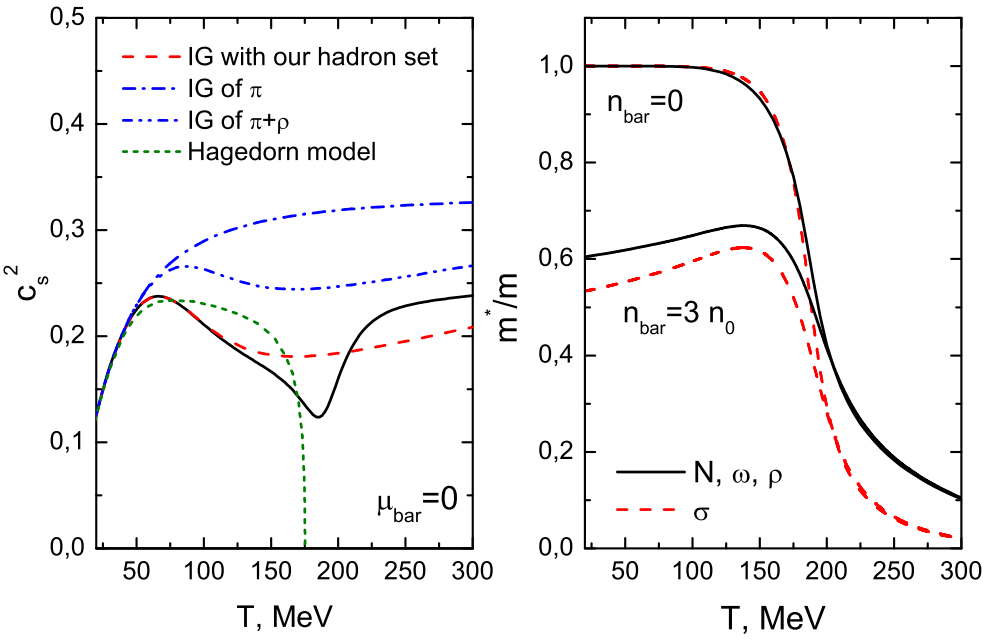

Fig. 1. Left panel: The sound speed squared in hadron matter as a function of the temperature at zero baryon chemical potential. Solid line – calculation within the SHMC model. Long-dashed line – calculation for the ideal gas of particles performed with the same hadron set. Dash-dotted and dash-double-dotted lines are results for the purely pion ideal gas and ideal pion-rho gas, respectively. Calculation results within the Hagedorn gas model [61,62] are plotted by the short-dashed line. Right panel: Temperature dependence of effective masses for nucleon, ω- and ρ-excitations (solid line) and the σ-meson excitation (dashed line) within the SHMC model for two values of the baryon density.

decrease of c_s^2, contrary to the case of the one-component pion gas. At still higher temperatures heavier species start to contribute in the case of multi-component systems resulting in a minimum in $c_s^2(T)$ for IG (see also [62]) and SHMC models. In the temperature range 50 MeV $< T <$ 150 MeV the decrease rate of c_s^2 is slower in the Hagedorn model than in the SHMC and IG models. Only for $T \approx T_H >$ 150 MeV a Hagedorn regime is reached, in which more and more energy goes into forming massive resonances and therefore, finally c_s^2 drops to zero. As mentioned above, the use of the suppressed coupling constants $g_{\sigma b}$, except for nucleons, guarantees that at $T_c < T < (220 \div 230)$ MeV the SHMC model results for the pressure are in agreement with the lattice results [58]. Within the SHMC model with this modification, c_s^2 gets a deep and rather narrow minimum at a critical point $T \approx T_c \simeq 180$ MeV [3] caused by a sharp decrease of the in-medium hadron masses at these temperatures

[3] The minimum of the speed of sound (at $T = T_c \simeq 180$ MeV) can be associated with a kind of phase transition, e.g. with the hadron-QGP crossover, as it follows from the detailed analysis of the lattice data, see [63].

(see the right panel in Fig. 1, where effective masses of the nucleon, ω-, ρ- and σ-excitations are presented). Note that in the m-truncated Hagedorn-gas model, c_s^2 remains finite at $T = T_H \approx T_c$: For $m < M = (1.5 \div 2.5)$ GeV the results [62] become very close to those for the IG model presented in Fig. 1. The specific behavior $c_s^2 \to 0$ arises in the Hagedorn model only for $m \to \infty$.

3 The HQB model

For the QGP phase of the IG of the massive quarks, antiquarks and gluons $\{q\} = q, \bar{q}, g$, see [56] we define the density of conserving charges similarly to Eqs. (20), (21):

$$n_{\rm bar}^{\rm HQB}(T, \mu_{\rm bar}, \mu_{\rm str}) = \sum_{a \in \{q\}} b_a \; n_a^{\rm IG}(T, \mu_a) \; , \tag{27}$$

$$n_{\rm str}^{\rm HQB}(T, \mu_{\rm bar}, \mu_{\rm str}) = \sum_{a \in \{q\}} s_a \; n_a^{\rm IG}(T, \mu_a) \; . \tag{28}$$

With nonperturbative effects associated with the deconfinement transition included into a constant vacuum pressure B, the total energy density and the pressure become

$$\varepsilon^{\rm HQB}(T, \mu_{\rm bar}, \mu_{\rm str}) = \sum_{a \in \{q\}} \varepsilon_a^{\rm IG}(T, \mu_a) + B \; , \tag{29}$$

$$P^{\rm HQB}(T, \mu_{\rm bar}, \mu_{\rm str}) = \sum_{a \in \{q\}} P_a^{\rm IG}(T, \mu_a) - B \; , \tag{30}$$

where for gluons ($a = g$) $\nu_g = 16$. The gluon chemical potential $\mu_g = 0$; thereby, gluonic energy density ε and pressure P depend only on temperature.

Effective masses of quarks and gluons are generally assumed to be temperature and density independent and are treated here as free parameters. From the fit of thermodynamic quantities to available lattice data for the $N_f = 2 + 1$ system [63,64,65] we get quark masses $m_u = m_d = 100$ MeV, $m_s = 450$ MeV and $m_g = 600$ MeV at $B = (215 \text{ MeV})^4$.

4 Equation of state in the two-phase model

Following a common strategy of the two-phase model [66], we determine here the deconfinement phase transition by matching the EoS of the SHMC model and the HQB model for quarks and gluons.

The phase equilibrium between the QGP and the hadronic phase at the first order phase transition is determined by the Gibbs conditions for thermal ($T^{\rm HQB} = T^{\rm SHMC}$), mechanical ($P^{\rm HQB} = P^{\rm SHMC}$) and chemical ($\mu_{\rm bar}^{\rm HQB} = \mu_{\rm bar}^{\rm SHMC}$, $\mu_{\rm str}^{\rm HQB} = \mu_{\rm str}^{\rm SHMC}$) equilibrium. The chemical equilibrium between different components is automatically satisfied owing to representation (26) for the chemical potential. At given temperature T and baryon chemical potential $\mu_{\rm bar}$ the strangeness chemical potential $\mu_{\rm str}$ is determined by fixing the net strangeness of the system to zero. So, in the Gibbs mixed phase at the fixed total baryon charge density $n_{\rm bar}$ the following set of equations is to be solved :

$$
\begin{aligned}
&P^{\rm SHMC}(T,\mu_{\rm bar},\mu_{\rm str}) = P^{\rm HQB}(T,\mu_{\rm bar},\mu_{\rm str}) \ , \\
&n_{\rm bar}(T,\mu_{\rm bar},\mu_{\rm str}) = \alpha \ n_{\rm bar}^{\rm HQB}(T,\mu_{\rm bar},\mu_{\rm str}) + (1-\alpha) \ n_{\rm bar}^{\rm SHMC}(T,\mu_{\rm bar},\mu_{\rm str}) \ , \\
&0 = \alpha \ n_{\rm str}^{\rm HQB}(T,\mu_{\rm bar},\mu_{\rm str}) + (1-\alpha) \ n_{\rm str}^{\rm SHMC}(T,\mu_{\rm bar},\mu_{\rm str}) \ ,
\end{aligned}
\tag{31}
$$

where $\alpha = V^{\rm HQB}/V$ is a volume fraction occupied by plasma, *i.e.* the coexistence phase is not a homogeneous one. The boundaries of this mixed phase are found by putting $\alpha = 1$ (*the hadron phase boundary*) and $\alpha = 0$ (*the plasma phase boundary*). Eqs. (31) should be solved at every phase point $(T, n_{\rm bar})$ of the coexistence region. It results in that the quark-hadron boundary of a system conserving baryon charge and strangeness becomes a critical surface (not a line in the $T - \mu_{\rm bar}$ plane as for a single charge conservation, but some stretched-out area [67].)

Predictions of the hadronic SHMC model with suppressed couplings agree with the recent lattice data for the reduced energy and the pressure up to about $T \simeq 220 \div 230$ MeV (see Fig. 2, left and right). As follows from Fig. 2, at higher temperatures quark-gluon degrees of freedom should be taken into account. Thereby, further we use the SHMC-HQB mixed phase model. In the $\mu_{\rm bar} = 0$ case the energy density of the SHMC-HQB mixed phase model suffers a jump at the temperature $T = T_c \approx 180$ MeV (the left panel in Fig. 2). This value of the critical temperature is consistent with that calculated on the lattice at $n_{\rm bar} = 0$ [64,68]. However the lattice data demonstrate a sharp crossover transition at this point. We found a jump in the latent heat about $\Delta\varepsilon \sim 0.85$ GeV/fm^3 ($\Delta\varepsilon/T^4 \sim 6$). The presence of the jump in ε at T_c indicates the first order phase transition. From the right panel of Fig. 2 we see that the pressure undergoes a continuous monotonous increase in temperature

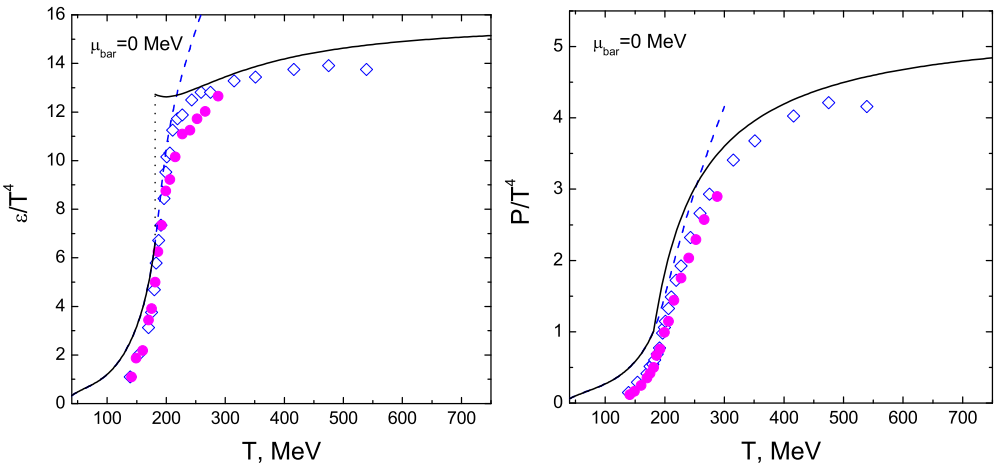

Fig. 2. Reduced energy density and pressure at $\mu_{\rm bar} = 0$ obtained in the two-phase SHMC-HQB model. The energy density jump at $T_c \approx 180$ MeV marked by the dotted line corresponds to the mixed phase. The hadronic SHMC results above T_c are plotted by dashed lines. QCD lattice results with the time extent N_t =8 for the p4 and asqtad actions are plotted by empty diamonds and filled circles, respectively [68].

in agreement with the construction of the mixed phase.

In Fig. 3 we demonstrate the reduced entropy density as a function of temperature. The lattice data using two types of the action are plotted by points for N_t =8. The results of the two-phase model and purely hadronic SHMC model are shown by solid and dashed (prolonged for $T > T_c$) lines, respectively. The SHMC model with suppressed couplings continues to be in close agreement with the lattice data till T ∼230 MeV. The HQB model agrees reasonably with the lattice data [68] for all temperatures above T_c except a narrow vicinity of the critical point where in the lattice QCD we deal with the crossover at $\mu_{\rm bar}$ =0.

Reasonable agreement between the SHMC-HQB model and lattice data is observed not only for the reduced energy, pressure and entropy but also for the trace anomaly $(\varepsilon - 3P)/T^4$, for both zero and finite values of the baryon chemical potentials, as demonstrated in the left and right panels of Fig. 4. As is seen, only at large temperatures $(\varepsilon - 3P)/T^4 \to 0$, i.e. the system becomes a conformal one. The conformal invariance in QCD is essentially broken at $T \lesssim 2T_c$. Therefore, we may expect here differences in predictions of conformal theories for different quantities, e.g. for η/s, at $T \lesssim 2T_c$. We stress that the conformal regime is not reproduced by the purely hadronic SHMC model, valid roughly for $T \lesssim 230$ MeV.

Values of the ratio P/ε and the speed of sound c_s essentially determine the evolution of a system, and as it will be shown below, the last quantity is

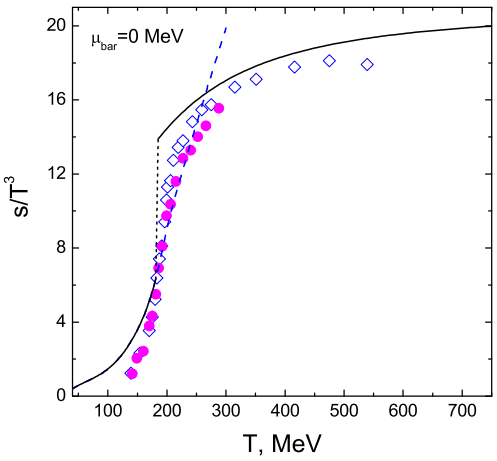

Fig. 3. Reduced entropy density at $\mu_{\rm bar} = 0$ obtained in the two-phase SHMC-HQB model. The entropy density jump at $T_c \approx 180$ MeV marked by the dotted line corresponds to the mixed phase. Notation is the same as in Fig. 2.

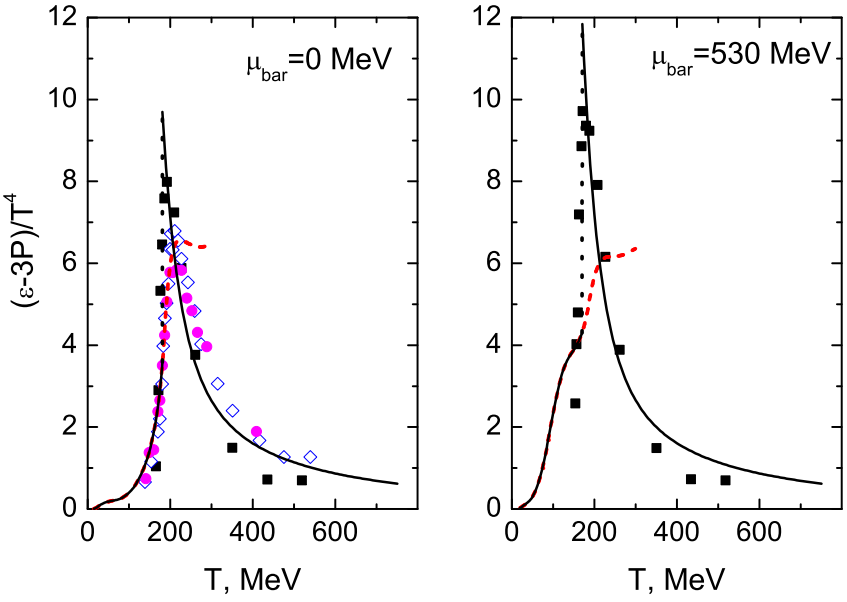

Fig. 4. Trace anomaly at $\mu_{\rm bar} = 0$ and $\mu_{\rm bar} = 530$ MeV. The jump is marked by the dotted line. The hadronic SHMC results are plotted above T_c by dashed lines. Lattice QCD data are from [69] (filled squares), and from [68] (circles and diamonds, notation is as in Fig. 2).

an important ingredient entering into the expression for the bulk viscosity coefficient.

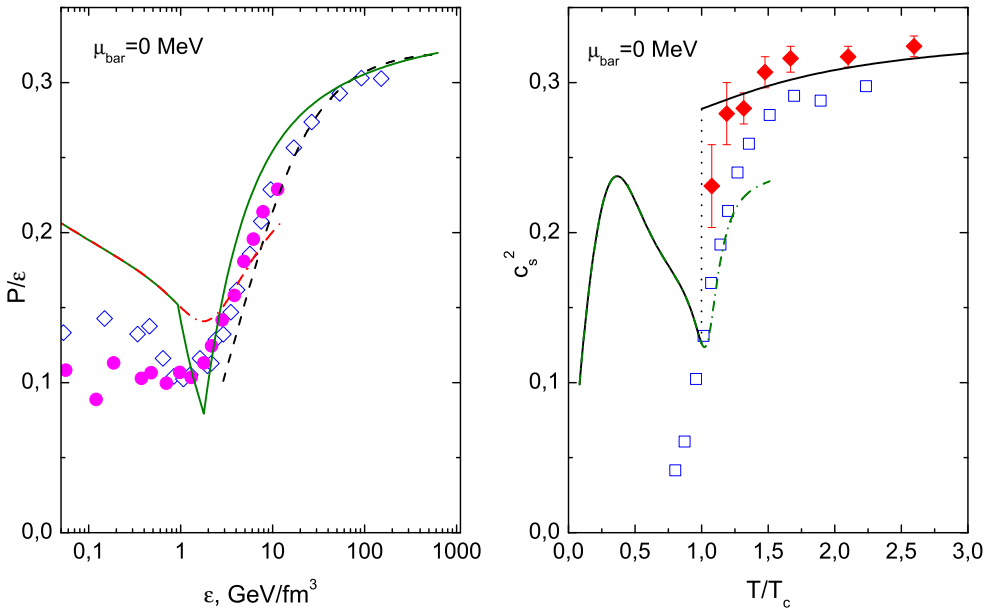

Fig. 5. The P/ε ratio demonstrating the presence of the softest point and the speed of sound squared in the baryonless matter are presented. Solid lines in both panels are results of our two-phase model calculations. Dash-dotted lines continuing the solid lines at $T > T_c$ demonstrate calculation results of the SHMC model. Left: empty diamonds and filled circles are the N_f =2+1 lattice data for the P/ε ratio calculated with the p4 and asqtad actions, respectively [68]. The dashed line is the high-T approximation (32) of lattice data with improved staggered fermions and almost physical masses for $N_f = 2 + 1$ [64]. Right: Diamonds and squares are lattice QCD data for N_f =2 with Wilson fermions [63] and N_f =2+1 with staggered fermions [70], respectively.

In Fig. 5 the energy density dependence of the P/ε ratio for the given two-phase SHMC-HQB model EoS is presented alongside with the temperature dependence of c_s^2. Both quantities (P/ε and c_s^2) have close physical meaning and coincide in the ultrarelativistic limit $c_s^2 = P/\varepsilon = 1/3$. This limiting trend is observed in Fig. 5 (left and right panels) at high temperatures and energies. In the high energy density region the SHMC-HQB results agree reasonably well with the lattice data. Though the cited above lattice results were obtained in different discretization schemes for 2- and (2+1) flavor QCD using different quark masses and lattice spacing, thermodynamics in the high temperature phase is not strongly influenced by discretization errors and is rather insensitive to changes of the quark mass. Nevertheless, one should be cautious treating these lattice QCD results for not too high temperatures, especially for $T < T_c$. Thereby, our point here is to use the HQB model for $T > T_c$ that fits the lattice results well for $T \gtrsim 2T_c$ and to apply our SHMC model in the hadronic sector at $T < T_c$, instead of using the corresponding lattice values for $T \lesssim T_c$. It is of interest to note that the SHMC model reasonably reproduces both P/ε and v_s^2 at the temperature above T_c till about 230 MeV,

in agreement with results presented in Figs. 2,3,4.

Lattice data [64] on the P/ε ratio obtained for the pion mass $m_\pi \approx 220$ MeV are well approximated in the high temperature/energy range $1.3 \lesssim \varepsilon^{1/4} \lesssim 6$ GeV/fm^3 as

$$\frac{P}{\varepsilon} = \frac{1}{3}\left(0.964 - \frac{1.16}{1 + 0.26\ \varepsilon\ \mathrm{fm}^3/\mathrm{GeV}}\right)\ . \tag{32}$$

This approximating curve is plotted by the dashed line in Fig. 5 (left panel). We see that different lattice data presented in this figure agree rather well with each other. Since $c_s^2 = dP/d\varepsilon$, the approximation (32) can also be used to reproduce the speed of sound. It is seen that in contrast with a single component hadronic gas (cf. Fig. 1 and Fig. 5), both c_s^2 and P/ε exhibit a minimum near the phase transition. In other words, the EoS in our two-phase SHMC-HQB model is getting softer near T_c and the system evolves slower at the "softest point", i.e. at the minimum of the P/ε ratio. As was noted above, for hadronic sector $T < T_c$ the lattice results predict much lower values of the P/ε ratio, as compared to our SHMC model. Being in discrepancy with lattice results for the low-temperature hadronic component, results of our two-phase and SHMC models agree reasonably well with other hadronic models, as it is demonstrated in Fig. 1.

The following remarks are in order. As was found within the standard RMF model [71] the specific heat exhibits a sign of critical behavior. The SHMC model with the standard choice of couplings demonstrates a crossover at a pseudocritical temperature $T \sim T_c$ for $\mu_{\rm bar} = 0$ in agreement with the lattice data. In this case we observe a sharp peak in the heat capacity which is typical for the strong crossover transition [57]. In our case when g_{mb} couplings are suppressed, the peak is smoothed that reminds about a weak crossover. Our two-phase SHMC-HQB model shows the first order phase transition. This can be treated as an advantage of the SHMC model and a disadvantage of the two-phase model. However the results of the SHCM model begin to disagree with the lattice data for $T > 220 - 230$ MeV, whereas the two-phase model fits well the lattice data in the high temperature region. Thus we can't use the SHMC model for high temperatures without its significant modification. We refuse of doing such a modification bearing in mind that the high temperature regime should be treated in terms of the quark-gluon degrees of freedom. The mentioned lack of our two-phase model can be removed by a more careful treatment of the near-critical region. On the one hand, in the framework of the model with the first-order phase transition our consideration of the vicinity of the critical point is obviously oversimplified, since the Gibbs condition's treatment disregards dynamical effects in the phase transition. The latter effects

are important for the description of the vicinity of the critical end point. These dynamical effects are manifested at temperature below the critical end point in all models with the EoS of the van der Waals type, see [54,72]. In particular, an overcooled state to be possibly formed at the first order phase transition may result in a mechanism of fast hadronization [73]. Thus one way to better treat the near-critical region is to incorporate non-trivial dynamical effects, e.g. in the framework of the van der Waals model EoS. On the other hand, one could smooth the thermodynamic quantities in the near-critical region in such a way that the EoS would correspond to the crossover for sufficiently small values of $\mu_{\rm bar}$, see [74]. We will return to the consideration of the critical effects in the subsequent work.

5 Shear and bulk viscosities in the hadron phase

5.1 Collisional viscosity in the SHMC model. Derivation of equations

Following Sasaki and Redlich [59], we derive expressions for the shear and bulk viscosities in the case when the quasiparticle spectrum is given by the expression $E(\vec{p}) = \sqrt{\vec{p}^{\,2} + m^{*\,2}(T,\mu)}$. We perform a similar derivation, but in the presence of mean fields σ and ω_0. In the latter case one should additionally take into account that quasiparticle distributions depend on the mean fields.

We start with the expression for the energy-momentum tensor:

$$T^{\mu\nu} = T^{\mu\nu}_{\rm MF} + \sum_{b\in\{\rm bar\}} T^{\mu\nu}_{b} + \sum_{\rm bos\in\{ex\}} T^{\mu\nu}_{\rm bos}, \tag{33}$$

where the mean-field contribution is as follows

$$T^{\mu\nu}_{\rm MF} = \left(\frac{1}{2} \left[m^{*\,2}_{\sigma}\ \sigma^2 - m^{*\,2}_{\omega}\ \omega_0^2 \right] + U(\sigma) \right) g^{\mu\nu}, \tag{34}$$

with m^*_σ and m^*_ω given by Eq. (6), and where we dropped the terms quadratic in gradients.

The quasiparticle (fermion and boson excitation) contribution is

$$T^{\mu\nu}_{a} = \int d\Gamma \left\{ \frac{(p^\mu_a + X^\mu_a) p^\nu_a}{E_a} F_a \right\}. \tag{35}$$

Here

$$p_a^\mu = (E_a(\vec{p}_a, \vec{r}_a), \vec{p}_a), \quad d\Gamma = \nu_a \frac{d^3 p_a}{(2\pi)^3}, \tag{36}$$
$$X_b^\mu = g_{\omega b}\ \chi_\omega\ \omega^\mu, \quad X_{\rm ex}^\mu = g^*_{\omega,{\rm ex}}\ \omega^\mu.$$

Note that the contribution to the energy-momentum tensor $T_a^{\mu\nu}$ is not symmetric with respect to the interchange of indices. The tensor can be symmetrized following a general rule, e.g. see [75]: One may add to $T^{\mu\nu}$ an extra term $T'^{\mu\nu}$, such that $\partial_\mu T'^{\mu\nu} = 0$ and that $T^{\mu\nu} + T'^{\mu\nu} = T^{\nu\mu} + T'^{\nu\mu}$. Thus the asymmetry of $T_a^{\mu\nu}$ does not influence on observables. In addition, to calculate viscosities we need to deal only with spatial components of the tensor, T^{ik}. Since $X^\mu = (X_0, 0, 0, 0)$ in the mean field approximation used by us, up to second gradients we have $T_a^{ik} \simeq T_a^{ki}$. Therefore we will not perform this symmetrization procedure in the given paper.

The quasiparticle distribution function F_b for baryon components in the presence of mean fields fulfills the Boltzmann kinetic equation [76],

$$\left(p_b^\mu \partial_\mu - g_{\omega b} p_\mu \omega^{\mu\nu} \frac{\partial}{\partial p_b^\nu} + m_b^* \partial^\nu m_b^* \frac{\partial}{\partial p_b^\nu} \right) \widetilde{F}_b = St\widetilde{F}_b; \tag{37}$$

with $\widetilde{F}_b(p_b, x_b) = \delta(p_b^2 - m_b^{*\,2}) F_b^{\rm loc.eq.}(\vec{p}_b, x_b)$.

The local equilibrium boson or baryon distribution is given as follows:

$$F_a^{\rm loc.eq.}(\vec{p}_a, x_a) = \left[e^{(E_a - \vec{p}_a \vec{u} - \mu_a + t_a^{\rm vec} X_a^0)/T} \pm 1 \right]^{-1}, \quad X_a^0 = g_{\omega a}\ \chi_\omega\ \omega_0, \tag{38}$$

where we suppressed $\vec{u}^{\,2}$ terms for $|\vec{u}| \ll 1$. [4] Here the upper sign $(+)$ is for fermions and $(-)$ is for bosons, and the vector particle charge is $t_a^{\rm vec} = \pm 1$ or 0; $g_{\omega a} \neq 0$ only for $a \in$ bar and kaons in our model. Considering only slightly inhomogeneous solutions and using $|\vec{u}| \ll 1$ we may drop the terms $\propto \vec{u}^2$ and $\propto \vec{u}\nabla\omega_0$ in the kinetic Eq. (37). Then kinetic equations for boson and baryon components acquire ordinary quasiparticle form

$$\frac{\partial F_a}{\partial t} + \frac{\partial E_a}{\partial \vec{p}_a}\frac{\partial F_a}{\partial \vec{r}_a} - \frac{\partial E_a}{\partial \vec{r}_a}\frac{\partial F_a}{\partial \vec{p}_a} = \frac{p_a^\mu}{E_a}\ \frac{\partial F_a}{\partial x_a^\mu} = St F_a, \tag{39}$$

[4] For $\vec{u} \neq 0$ there appear mean field solutions with $\vec{\omega} \neq 0$. These however yield $\vec{u}^{\,2} \ll 1$ terms.

where $p_a^\mu = (E_a(\vec{p}_a, \vec{r}_a, \sigma, \omega), \vec{p}_a)$. We used that $\partial E_a/\partial \vec{p}_a = \vec{p}_a/E_a$. Since calculating the viscosity, we need only terms with velocity gradients, we further put $\partial E_a/\partial \vec{r}_a = (\partial E_a/\partial \mu_a)\vec{\nabla}_a \mu_a + (\partial E_a/\partial T)\vec{\nabla}_a T = 0$.

In the relaxation time approximation

$$StF_a = -\delta F_a/\tau_a, \quad \delta F_a = F_a - F_a^{\rm loc.eq.}. \tag{40}$$

Here τ_a denotes the relaxation time of the given species. Generally, it depends on the quasiparticle momentum $\vec{p}_a$.

The averaged partial relaxation time $\tilde{\tau}_a$ is related to the cross section as

$$\tilde{\tau}_a^{-1}(T,\mu) = \sum_{a'} n_{a'}(T,\mu) \left\langle v_{aa'} \sigma^t_{aa'}(v_{aa'}) \right\rangle, \tag{41}$$

where $n_{a'}$ is the density of a'-species, $\sigma^t_{aa'} = \int d\cos\theta \, d\sigma(aa' \to aa')/d\cos\theta \, (1-\cos\theta)$ is the transport cross section, in general, accounting for in-medium effects and $v_{aa'}$ is the relative velocity of two colliding particles a and a' in case of binary collisions. Angular brackets denote a quantum mechanical statistical average over an equilibrated system. In reality, the cross sections entering the collision integral and the corresponding relaxation time τ_a in (40) may essentially depend on the particle momentum. Thus, averaged values $\tilde{\tau}_a^{-1}$ given by Eq. (41) yield only a rough estimate for the values τ_a^{-1} which we actually need for calculation of viscosity coefficients, see below Eqs. (48) and (49).

In the relaxation time approximation from Eqs. (39), (40) we obtain

$$\delta F_a = -\frac{\tau_a}{E_a} \, p_a^\mu \, \frac{\partial F_a^{\rm loc.eq.}}{\partial x_a^\mu}, \tag{42}$$

and then the nonequilibrium correction to the energy-momentum tensor (33) becomes:

$$\begin{aligned} \delta T^{\mu\nu} = &- \sum_a \int d\Gamma \left\{ \tau_a \frac{(p_a^\mu + X_a^\mu) p_a^\nu}{E_a^2} \, p_a^\kappa \partial_\kappa F_a \right\}_{\rm loc.eq.} \\ &+ \delta\sigma \, \frac{\partial T^{\mu\nu}}{\partial \sigma}_{\rm loc.eq.} + \delta\omega_0 \, \frac{\partial T^{\mu\nu}}{\partial \omega_0}_{\rm loc.eq.}. \end{aligned} \tag{43}$$

Considering small deviations from the local equilibrium, we may keep in (43) only first-order derivative quasiparticle terms $\propto \partial_\mu$.

The shear and bulk viscosities expressed through traceless nondiagonal and diagonal parts of the nonequilibrium correction to the energy-momentum tensor are as follows:

$$\delta T_{ij} = -\zeta\ \delta_{ij}\vec{\nabla}\cdot\vec{u} - \eta\ W_{ij}, \qquad (44)$$
$$W_{kl} = \partial_k u_l + \partial_l u_k - \frac{2}{3}\delta_{kl}\ \partial_i u^i.$$

As before, here Latin indices run $1, 2, 3$.

To find the shear viscosity, we put $i \neq j$ in (44) and use that in this case the variation of the second and third terms in (43) yields zero after integration over angles. To find the bulk viscosity, we substitute $i = j$ in (44) and use that $T^{ii}_{\rm eq} = 3P_{\rm eq}$. As follows from equations of motion (11), variation of the second and third terms in (43) again yields zero. We put $\vec{u} = 0$ in final expressions but retain gradients of the velocity.

Taking derivatives $\partial F_a^{\rm loc.eq.}/\partial x_a^\mu$ in Eq. (42) with the help of Eqs. (79) – (81) from Appendix A, we find the variation of the total energy-momentum tensor as the function of derivatives of the velocity [5]

$$\delta T^{ij} = \sum_a \int d\Gamma\ \frac{p_a^i p_a^j}{T E_a}\,\tau_a\ F_a^{\rm eq}(1 \mp F_a^{\rm eq})\, q_a(\vec{p}; T, \mu_{\rm bar}, \mu_{\rm str}) \qquad (45)$$

with the upper sign $(-)$ in the blocking factor for fermions and the lower one $(+)$ for bosons in accordance with Eqs. (25),(38),

$$q_a(\vec{p}; T, \mu_{\rm bar}, \mu_{\rm str}) = \partial_k u_l\ \delta_{kl}\ Q_a - \frac{p_k p_l}{2E_a}\ W_{kl}, \qquad (46)$$

$$\begin{aligned} Q_a = -\Bigg\{ & \frac{\vec{p}_a^{\,2}}{3E_a} + \left(\frac{\partial P}{\partial n_{\rm bar}}\right)_{\epsilon, n_{\rm str}} \left[\frac{\partial(E_a + X_a^0)}{\partial \mu_{\rm bar}} - t_b^{\rm bar}\right] \\ & + \left(\frac{\partial P}{\partial n_{\rm str}}\right)_{\epsilon, n_{\rm bar}} \left[\frac{\partial(E_a + X_a^0)}{\partial \mu_{\rm str}} - t_a^{\rm str}\right] - \left(\frac{\partial P}{\partial \epsilon}\right)_{n_{\rm bar}, n_{\rm str}} \\ & \times \left[E_a + X_a^0 - T\frac{\partial(E_a + X_a^0)}{\partial T} - \mu_{\rm bar}\frac{\partial(E_a + X_a^0)}{\partial \mu_{\rm bar}} - \mu_{\rm str}\frac{\partial(E_a + X_a^0)}{\partial \mu_{\rm str}}\right]\Bigg\}. \end{aligned} \qquad (47)$$

[5] Since we are not interested in calculations of the heat conductivity, we again suppress the $\vec{\nabla}T$, $\vec{\nabla}\mu$ terms and also put $\vec{u} = 0$ keeping only the corresponding derivative terms.

Finally, we obtain the shear viscosity

$$\eta = \frac{1}{15T}\sum_a \int d\Gamma\, \tau_a \frac{\vec{p}_a^{\,4}}{E_a^2}\, \left[F_a^{\rm eq}\,(1 \mp F_a^{\rm eq})\right]. \tag{48}$$

Correspondingly, the bulk viscosity is

$$\zeta = -\frac{1}{3T}\sum_a \int {\rm d}\Gamma\, \tau_a\, \frac{\vec{p}_a^{\,2}}{E_a}\, F_a^{\rm eq}\, \left(1 \mp F_a^{\rm eq}\right) Q_a. \tag{49}$$

To get a final expression for the latter quantity, one should use the energy conservation obtained from Eq. (45) by demanding $\delta T^{00} = 0$,

$$\sum_a \int d\,\Gamma\, \Big[\tau_a\,(E_a + X_a^0)\, F_a^{\rm eq}\,(1 \mp F_a^{\rm eq})\, q_a + \bar{\tau}_a\,(E_a - X_a^0)\, \bar{F}_a^{\rm eq}\,(1 \mp \bar{F}_a^{\rm eq})\, q_{\bar{a}}\Big] = 0\ , \tag{50}$$

where the second term corresponds to antiparticles with the relaxation time $\bar{\tau}_a$. After substitution of Eq. (50) in (49), the bulk viscosity can be presented as

$$\begin{aligned}\zeta = &-\frac{1}{3T}\sum_a \int {\rm d}\Gamma\, \left(-\frac{m_a^{*2}}{E_a} - X_a^0\right) \tau_a\, F_a^{\rm eq}\,(1 \mp F_a^{\rm eq})\; Q_a \\ &-\frac{1}{3T}\sum_a \int {\rm d}\Gamma\, \bar{\tau}_a \left(-\frac{m_a^{*2}}{E_a} + X_a^0\right) \bar{F}_a^{\rm eq}\, \left(1 \mp \bar{F}_a^{\rm eq}\right)\, Q_{\bar{a}},\end{aligned} \tag{51}$$

where Q_a is defined by Eq. (47).

For $X_a^0 = 0$, $\mu_{\rm str} = 0$ our results coincide with those obtained in [59]:

$$\eta_a = \frac{1}{15T}\int d\Gamma\, \tau_a \frac{\vec{p}_a^{\,4}}{E_a^2}\, \left[F_a^{\rm eq}\,(1 \mp F_a^{\rm eq})\right], \tag{52}$$

$$\begin{aligned}\zeta_a = &-\frac{1}{3T}\int {\rm d}\Gamma\, \tau_a \frac{m_a^{*2}}{E_a}\, F_a^{\rm eq}\,(1 \mp F_a^{\rm eq})\; \times \\ &\times \left\{\frac{\vec{p}_a^{\,2}}{3E_a} + \left(\frac{\partial P}{\partial n_{\rm bar}}\right)_{\epsilon, n_{\rm str}} \left[\frac{\partial E}{\partial \mu_{\rm bar}} - t_b^{\rm bar}\right]\right. \\ &\left. - \left(\frac{\partial P}{\partial \epsilon}\right)_{n_{\rm bar}, n_{\rm str}} \left[E_a - T\frac{\partial E_a}{\partial T} - \mu_{\rm bar}\frac{\partial E_a}{\partial \mu_{\rm bar}}\right]\right\}\end{aligned} \tag{53}$$

where the quasiparticle mass m_a^* can be temperature/density dependent. Making substitution of the on-shell mass instead of m_a^* and $F_a^{\rm eq} = F_a^{\rm IG}$ in Eqs. (52),

(53) we arrive at expressions for the gas of non-interacting particles. For the gas of quasiparticles with values m^* depending only on the temperature with the help of Eq. (50), Eq. (53) can be rewritten in a simpler form [16]

$$\zeta = \frac{1}{T}\int \mathrm{d}\Gamma\, \tau\, F^{\mathrm{eq}}\,(1 \mp F^{\mathrm{eq}})\,\left\{\left(\frac{1}{3} - c_s^2\right) E - \frac{m^{*2}}{3E}\right\}^2 . \tag{54}$$

In a particular case of the one component gas of material particles in the high temperature limit $T \gg m$ for $\tau = \tilde{\tau} = const$ viscosity coefficients take the simplest form [16]:

$$\eta \simeq \frac{4\tilde{\tau}}{15}\, e(T), \qquad\qquad \zeta \simeq 0, \tag{55}$$

where $e(T) = \frac{1}{30}\pi^2 T^4$ is the known black-body radiation result for a massless Bose fluid.

5.2 Collisional viscosity in hadronic baryonless matter

In the relaxation time approximation both shear and bulk viscosities for a component "a" depend on its relaxation (collisional) time τ_a, which should be parameterized or calculated independently. Therefore to diminish this uncertainty it is legitimate at first to find the reduced kinetic coefficients (per unit relaxation time, assuming $\tau = const$, i.e. $\tau = \tilde{\tau}$).

In Fig. 6 we demonstrate results of various calculations for the reduced shear (left panel) and bulk (right panel) viscosities at $\mu_{\mathrm{bar}} = 0$ additionally scaled by the $1/T^4$ factor. As we see from the figure, the reduced scaled shear viscosity of the massive pion gas (dashed line) becomes approximately constant for $T \gtrsim 100$ MeV. Naturally, this result is close to that obtained in the Gavin approximation [16] where a numerical interpolation between the $m/T \ll 1$ and $m/T \gg 1$ cases was used (dash-double-dotted line in Fig. 6). The T^4 scaling is violated for the $\pi - \rho$ gas in the temperature interval under consideration because the ρ mass is not negligible even at $T \sim 200$ MeV. For ζ the approximate $1/T^4$ scaling property holds for the massive pion-rho gas at $T \gtrsim 150$ MeV. Note that $\zeta = 0$ for the gas of free massless pions since $c_s^2 = 1/3$ in this case. For the massive pion gas ζ/T^4 gets maximum for $T \simeq 60$ MeV and then begins to decrease for $T > 60$ MeV reaching zero at large T similar to the case of massless gas. The reduced shear and bulk viscosities of a multicomponent system calculated in our SHMC model (solid lines) and in the IG model with

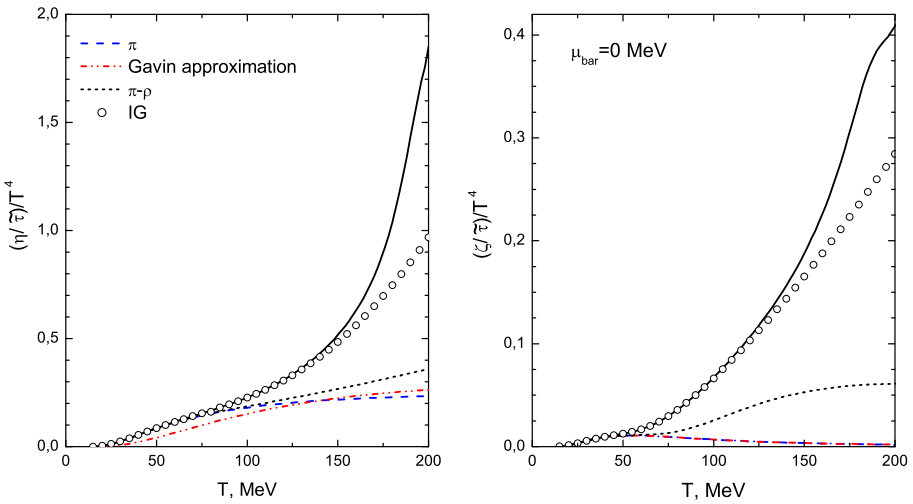

Fig. 6. The reduced T^4 scaled shear (left panel) and bulk (right panel) viscosities per unit relaxation time calculated within the SHMC model for a system with $\mu_{\rm bar}$ =0 (solid lines). The results are compared with those for the massive pion gas (dashed lines), $\pi - \rho$ mixture (short dashed line) calculations and with some interpolation from massive to massless pion gas (the Gavin approximation [16], dash-double-dotted line) as well as for the IG model with the same large set of species as in the SHMC model (open dots).

the same hadron set (open dots) do not fulfill the T^4 scaling law. These models include a large set of hadrons. Due to that with the temperature increase the reduced shear and bulk viscosities become significantly higher than those for the pion gas and the pion-rho gas models. An additional increase of the reduced viscosity within the SHMC model originates from significant mass decrease at temperatures near the critical temperature. The bulk viscosity of a single-component pion system drops to zero both at low and high temperatures and in the whole temperature interval $\zeta << \eta$, that is frequently used as an argument for neglecting the bulk viscosity effects. However, the statement does not hold anymore for mixture of many species. For example, at T ∼150 MeV the η/ζ ratio is only about 3 in the case of the IG and SHMC models. Thus the bulk viscosity effects can play a role in the description of the hadronic stage at high collision energies, like at RHIC. Moreover, the bulk viscosity can be responsible for such important effect as flow anisotropy.

For further evaluation of the absolute values of the transport coefficients η_a and ζ_a we need to estimate the relaxation time of hadronic species. For that we use Eq. (41). We apply free cross sections in the case of the IG based model, similar to procedure performed in Ref. [77]. For the SHMC model, the in-medium modification of cross sections is incorporated by a shift of a "pole" of the collision energy by the mass difference $m_a - m_a^*$ according to prescription of Ref. [78]. Due to a lack of microscopic calculations this is the

only modification, which we do here.

The relaxation time for the $\pi\pi$ collisions in the purely pion gas is plotted in Fig. 7. The same cross sections as in Ref. [77] are taken since pions within our SHMC model are assumed to have free dispersion law, as well as in Ref. [77]. Therefore our results (solid and dash curves) coincide with those in Ref. [77]

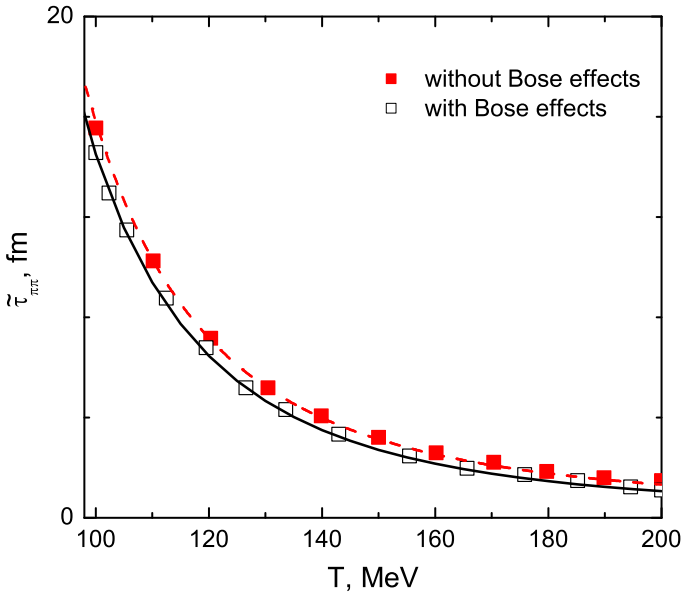

Fig. 7. The pion relaxation time for the $\pi\pi$ system as a function of temperature. Solid and dashed lines are our calculation results for quantum Bose and classical Boltzmann statistics, respectively. The corresponding points (empty and black squares) are taken from the review-article of Prakash et al. [77].

(empty and black squares). As is seen, there is only a small influence of quantum statistics on the pion relaxation time.

The temperature dependence of the ratio of transport coefficients to the entropy density is analyzed in Fig. 8 for the $\mu_{\rm bar}$ =0 system. Here we make emphasis on the high-T behavior to clarify the question how hadronic models describe approaching the lower bound of the $\eta/s = 1/4\pi$ ratio predicted by strongly coupled theories [21,25,31]. As is seen from Fig. 8 (left panel), the SHMC model (solid lines) as well as the excluded volume one (short dashed and dash-dotted lines) [79] predict a monotonous decrease of the specific shear viscosity η/s. However, only in the SHMC model the lower bound $\eta/s \sim 1/4\pi$ is reached at the critical temperature $T_c \approx 180$ MeV. The hadron model [80] describes all the known particles and resonances with masses $m_i < 2$ GeV in terms of an excluded volume model with $r = 0.5$ fm and additionally includes an exponentially increasing number of Hagedorn states for $m_i > 2$ GeV. It is natural that for $T \lesssim 140$ MeV the resonance gas model with the Hagedorn states reproduces the behavior of η/s for the hadron excluded volume model

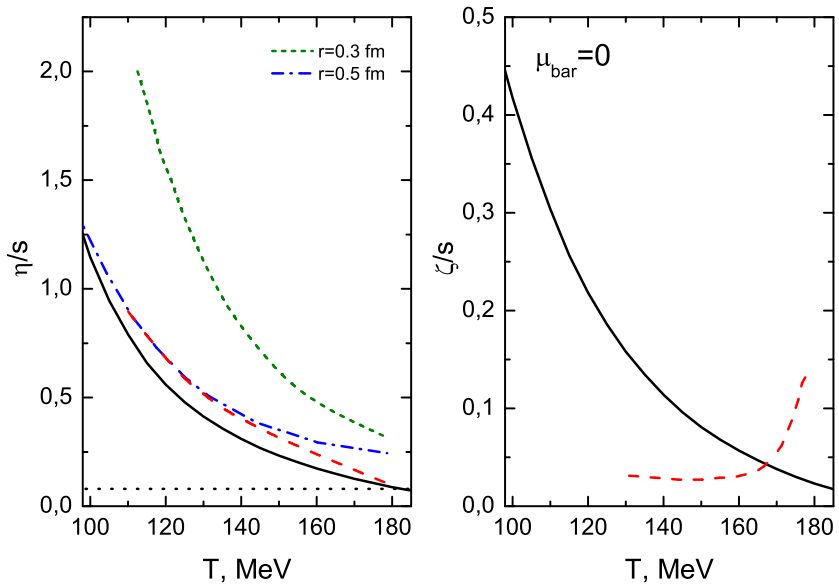

Fig. 8. Specific shear (left panel) and bulk (right panel) viscosities (η/s and ζ/s) of hadrons as a function of T for $\mu_{\rm bar}$ =0. Our SHMC model results are shown by solid lines. The results of the excluded volume hadron gas model [79] are shown for two values of hard-core radii r (short dashed and dash-dotted lines). The results for the resonance gas model including Hagedorn states [80] are shown by the long–dashed lines. The dotted horizontal line corresponds to the lower AdS/CFT bound, $\eta/s = 1/4\pi$ [31].

for $r = 0.5$ fm. At $T \sim T_c$ results for the shear viscosity calculated in the line of classical non-relativistic approximation [80] are consistent with the lower bound of the η/s ratio. Note that our SHMC relativistic mean-field model does not need extra assumptions on the particular Hagedorn states to describe the dip in c_s^2 and $\eta/s \sim 1/4\pi$ near the critical temperature.

The specific bulk viscosity ζ/s (see Fig. 8, right panel) behaves quite differently in our SHMC and the Hagedorn hadronic models since completely different assumptions were used for calculation of the bulk viscosity. Namely, our results are based on the quasiparticle collisional relaxation time approximation while in [80], following the QCD sum rules in [50,51], the bulk viscosity ζ was related with the trace anomaly $< \theta >_T \equiv < T^\mu_\mu >_T = \varepsilon - 3P$:

$$\zeta(T) = \frac{1}{9\omega_0(T)} \left[T^5 \frac{\partial}{\partial T} \frac{< \theta >_T - < \theta >_0}{T^4} + 16|\varepsilon_0| \right], \qquad (56)$$

where $|\varepsilon_0| = < \theta >_0 /4$ in vacuum. To derive Eq. (56), a particular ansatz was used for the spectral function at zero momentum. However, recently this ansatz has been criticized in [46,52,81,82]. Moreover, Eq. (56) obviously is not applicable for temperatures far from T_c.

Viscosities in the interacting hadronic phase were calculated in Ref. [83] for $T < T_c$ when the dominant configuration of QCD with two flavors of massless quarks is the interacting gas of chiral pions. In the large N_c limit for massless chiral pions it was obtained that

$$\left(\frac{\zeta}{\eta}\right)_\pi \sim \left(\frac{1}{3} - \frac{P}{\varepsilon}\right)\left(\frac{1}{3} - c_s^2\right) . \tag{57}$$

As was first shown by Gavin [16] in pure massless ideal pion gas $\zeta = 0$. However if pions are coupled with themselves or with the matter of other species $\varepsilon \neq 3P$ and $\zeta_\pi \neq 0$. Eq. (57) is similar to a simplified expression $\zeta/\eta \sim 15(\frac{1}{3} - c_s^2)^2$ which is obtained for a photon gas coupled to hot matter [84] and is also parameterically correct for perturbative QCD [45]. This is because $2 \to 2$ scattering is the dominant process in both η and ζ calculations. It is however not the case, *e.g.* in the $\lambda\phi^4$ model, where η is dominated by $2 \leftrightarrow 4$ processes while ζ by $2 \to 2$. For a strongly coupled $N = 2^*$ gauge theory using AdS/CFT [25] the scaling is $\zeta/\eta \propto (\frac{1}{3} - c_s^2)^2$.

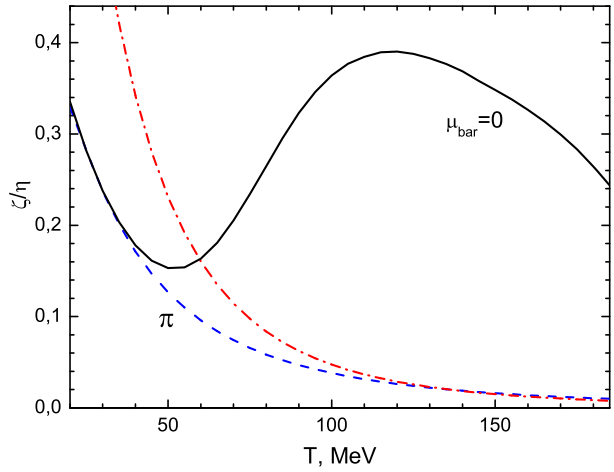

Fig. 9. The ratio of the bulk-to-shear viscosity for baryonless hadronic matter calculated within the SHMC model (solid line) and for the massive ideal pion gas (dashed line). For comparison T-dependence of the ratio calculated following Eq. (57) (i.e. as for chiral pions, but with thermodynamical quantities as for the massive ideal pion gas and normalized to the value for the massive pion gas at large T), is shown by the dash-dotted line.

In Fig. 9 we show the ratio ζ/η calculated for baryon-less matter in SHMC model (solid line) and those computed for the massive pion gas with a free dispersion law (dashed). For comparison the ζ/η-ratio calculated according to Eq. (57) (i.e., as for chiral pions) but with thermodynamic quantities the same as for the massive pion gas is shown by the dash-dotted line. At $T \gtrsim m_\pi$ pions become almost chiral ones and the T dependence of the pion gas

indeed can be described by Eq. (57). This coincidence of two curves at large T allowed us to estimate the value of the numerical pre-factor in Eq. (57). For $\mu_{\rm bar} = 0$ the ζ/η ratio in our SHMC model coincides at $T < 50$ MeV with that for the free massive pion gas. It demonstrates that the main contribution to viscosities is given here by the pion mode. In the purely pion case the ratio ζ/η monotonously decreases with increase of the temperature, whereas within our SHMC model it gets a minimum at $T \sim 50$ MeV and then a maximum for $T \sim 120$ MeV.

5.3 Collisional viscosity in baryon enriched hadronic matter

Similarly to the $\mu_{\rm bar}$ =0 case, to avoid influence of uncertainties in the value of the relaxation time we study at first reduced kinetic coefficients. Transport coefficients for a nucleon-antinucleon mixture at finite baryon density were calculated earlier by Hakim and Mornas within the standard Walecka model [11]. Comparison between their (dotted lines) and our (solid lines) SHMC model results is given in Fig.10 for two values of the density. Since Ref. [11] presented results for one component (neutron) matter, we performed calculations in the SHMC model also for neutron-antineutron matter. Because the ρ mean field is absent in the standard Walecka model, we suppressed the ρ-term also in the SHMC model calculation. We see that the reduced T^4-scaled shear viscosity behaves similarly in both models but absolute values differ due to different effective masses. Only at high temperatures and for $n_{\rm bar} \simeq n_0$ (n_0 is the nuclear saturation density) the values of reduced shear viscosities become close in both models. Differences in the values of the reduced bulk viscosity calculated in two models are larger than for the reduced shear viscosity because ζ depends on the specific behavior of thermodynamical quantities (cf. Eqs. (52) and (53)). In particular, it concerns the high-density region (see the curves for $n_{\rm bar} = 4n_0$), when the mass in the standard Walecka model is getting very small.

The temperature dependencies of the reduced T^4-scaled shear and bulk viscosities calculated for the case of the multi-component hadron mixture within IG and SHMC models are shown in the left and right panels of Fig. 11 at baryon densities $n_{\rm bar} = n_0$ and $4n_0$. The reduced shear viscosity calculated in the SHMC model (solid lines) is close to that in the IG model with the same hadron set (dashed lines). Differences in the $\eta/(\tau T^4)$ ratio for the IG and SHMC models appear only at high temperatures $T \gtrsim 150$ MeV. At $T \lesssim 100$ MeV the reduced T^4-scaled bulk viscosity (right panel) in the IG based model proved to be larger than that in the SHMC model. Contrary, for larger T the values of the reduced bulk viscosity in the IG model become smaller than those in the SHMC model. Differences come from the strong dependence of the bulk

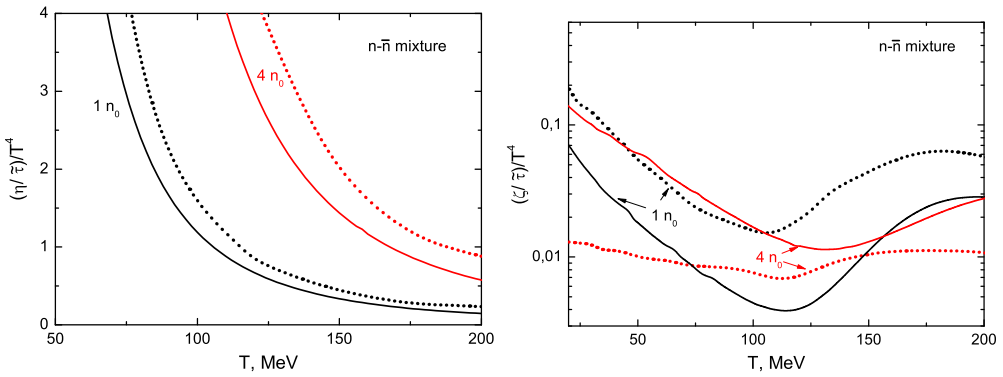

Fig. 10. The temperature dependence of the reduced T^4-scaled shear (left panel) and bulk (right panel) viscosities per unit relaxation time calculated for a one-component pure nucleon-antinucleon system at $n_{\rm bar} = n_0$ and $4n_0$. Solid lines are the SHMC model calculations. The standard Walecka model results [11] are plotted by dotted lines.

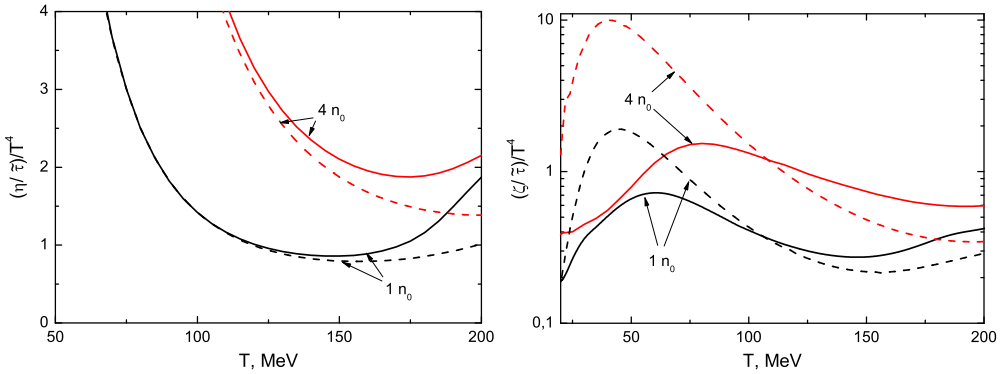

Fig. 11. The SHMC model predictions of the T^4-scaled temperature dependence of the reduced shear (left panel) and bulk (right panel) viscosities calculated for hadron mixture at $n_{\rm bar} = n_0$ and $4n_0$ (solid lines). Calculations performed in the IG based model with the same hadron set as in the SHMC model are demonstrated by dashed lines.

viscosity ζ on the values of thermodynamical quantities (see Eqs. (47), (49)). Note that at $T \gtrsim$100 MeV and $n_{\rm bar} \gtrsim n_0$ the shear and bulk viscosities are getting comparable in magnitude. Growth of the relative importance of ζ with increase of temperature seems to be quite natural because the bulk viscosity takes into account momentum dissipation due to inelastic channels and those number grows with the temperature increase.

Now let us proceed to an estimate of the relaxation time for a baryon enriched nuclear system. Important peculiarity of the nucleon contribution to the relaxation time at low temperature is associated with the particular role played by the Pauli blocking. It means that appropriate multi-dimensional integration should be carried out quite accurately with using quantum statistical distri-

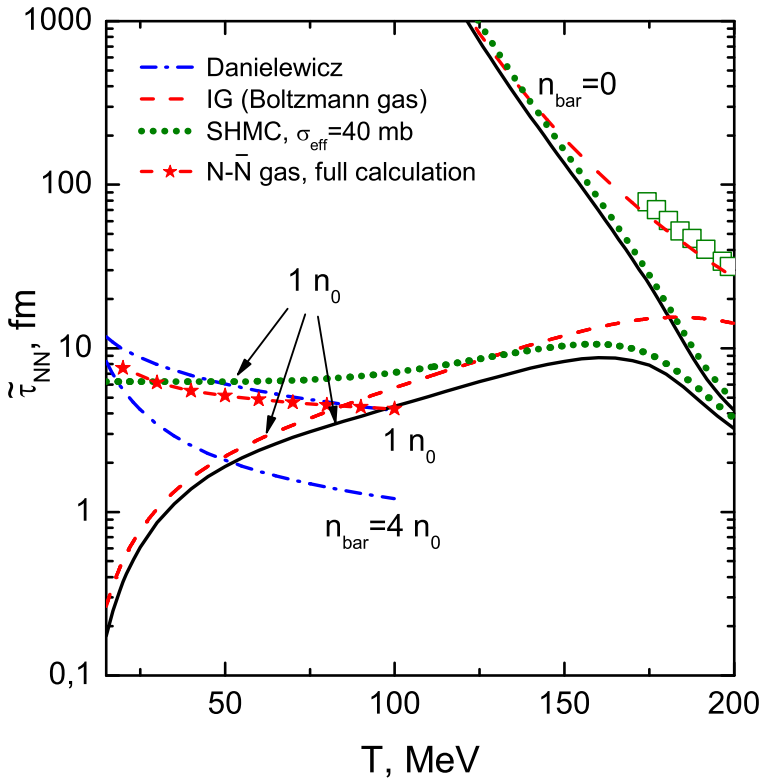

Fig. 12. The temperature dependence of the partial nucleon-nucleon relaxation time for $n_{\rm bar} = 0$ and $1n_0$. SHMC model calculations with the relativistic Boltzmann distribution function performed following (41) with the experimental free nucleon-nucleon cross section are shown by solid lines and those with the effective cross-section $\sigma_{NN} = \sigma_{eff}$ =40 mb, by dotted lines, respectively. The full calculation for nucleon component at $n = n_0$ performed with the Fermi distribution function is presented by stars. The ideal Boltzmann nucleon-antinucleon gas model results are shown by dashed curves. The Danielewicz interpolation given by Eq. (58) of [9] is plotted by dash-dotted lines for $1n_0$ and $4n_0$. Squares are results of calculations [77] for $n_{\rm bar} = 0$ performed within the Boltzmann approximation.

bution functions. Calculations using the kinetic Uehling-Uhlenbeck equations for the purely nucleon system ($N = Z$) in the non-relativistic approximation were performed in Ref.[9]. For $T \lesssim 100$ MeV an interpolated expression has been obtained:

$$\tilde{\tau}_{NN} \simeq \frac{850}{T^2}\left(\frac{n_{\rm bar}}{n_0}\right)^{1/3}\left[1+0.04T\frac{n_{\rm bar}}{n_0}\right]+\frac{38}{T^{1/2}(1+160/T^2)}\frac{n_0}{n_{\rm bar}}\ . \qquad (58)$$

Here $\tilde{\tau}_{NN}$ is in fm/c, T is in MeV, $n_0 = 0.145$ fm^{-3}. Thus the relaxation time demonstrates well known T^{-2} behavior for a Fermi liquid at $T \to 0$, cf. [85].

In Fig.12 we compare evaluation (58) with the relaxation time, as it follows

from the SHMC model for the purely nucleon-antinucleon system with $N = Z$. Here we use the Boltzmann approximation and free cross sections just corrected by the nucleon mass shift (see solid lines). As is seen from Fig.12, due to an account for the Pauli principle the Danielewicz's $\tilde{\tau}_{NN}$ given by Eq. (58) (see dash-dotted line) essentially deviates from the SHMC model result (computed here within Boltzmann approximation) for $T \lesssim 100$ MeV. The SHMC model results are very close to those for the ideal nucleon-antinucleon gas (dashed lines) for $T \lesssim 150$ MeV. A partial account of the Pauli principle by assuming constant effective cross section σ_{eff} =40 mb (see dotted line) improves SHMC model agreement with the estimates (58) at low T. Our full calculation of $\tilde{\tau}_{NN}$ for a purely nucleon gas that includes Pauli principle plotted by stars demonstrates a reasonable agreement with (58). Therefore to simplify calculations below we use Eq. (58) for the partial nucleon-nucleon relaxation time $\tilde{\tau}_{NN}$, to be valid at low temperatures, smoothly matching it (at $T \sim 100$ MeV) with the partial nucleon contribution calculated following Eq. (41) for higher temperatures. In the case $n_{\rm bar}$ =0 the ideal Boltzmann gas model results (dash curve) are very close to those of [77] (squares) and agree with the SHMC calculations (also performed in the Boltzmann approximation, see solid and dotted lines) for $T \lesssim 150$MeV. For higher T the difference with the IG model is due to a sharp change of the effective nucleon mass in the SHMC model at large temperatures.

In subsequent calculations we take into account the whole hadron set involved into the SHMC model. The relaxation time for every component, except for nucleons, is evaluated according to Eq. (41).

In Fig.13 (left) the partial contribution of the nucleon shear viscosity for the multi-component system is pictured as a function of temperature at $n_{\rm bar} = 1n_0$ and $4n_0$. Solid and dashed lines are our results for the SHMC and IG models, respectively, with the relaxation time calculated following Eq. (58). The dot-dashed lines show the Danielewicz analytical fit [9]

$$\eta \simeq (1700/T^2)\,(n_{\rm bar}/n_0)^2 + [22/(1+T^2\cdot 10^{-3})]\,(n_{\rm bar}/n_0)^{0.70} + 5.8T^{1/2}/(1+160/T^2)\,, \qquad (59)$$

where η is given in MeV/(fm^2c), T in MeV. For both $n_{\rm bar}/n_0$ =1 and 4 the IG model results are rather close to this fit, provided $\tilde{\tau}_{NN}$ is calculated according to (58). The shear viscosity calculated under the same conditions within the SHMC model is higher than that calculated following Eq. (59) and in IG model, since the former takes into account decrease of the effective masses with the increase of the baryon density. Two short-dashed curves at the bottom of Fig.13 (left) represent η computed in the SHMC model within the Boltzmann approximation for densities $n_{\rm bar} = n_0$ and $4n_0$. As is expected,

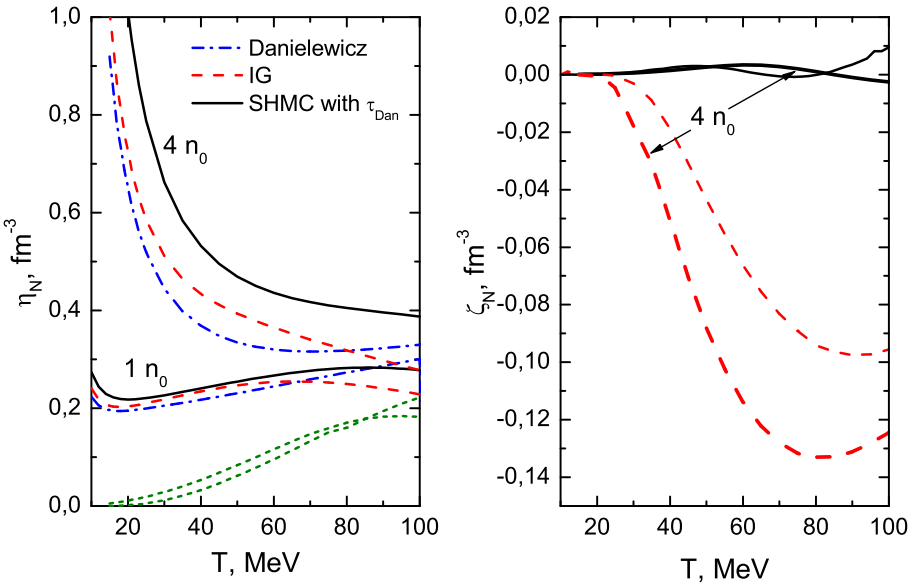

Fig. 13. The T-dependence of the partial nucleon contribution to the shear and bulk viscosity in the multi-component system for different values of the baryon density $n_{\rm bar}$. Solid and dashed lines are our results, respectively, for the SHMC and IG models with the same particle set, with the relaxation time calculated following Eq. (58). Dot-dashed curves are the Danielewicz interpolation (59) of results [9]. For comparison in left panel two short-dashed lines are shown for the SHMC model calculations done within the Boltzmann gas approximation at $n_{\rm bar} = 4n_0$ (upper line in low T region) and n_0. In right panel bold solid and dashed lines correspond to $n_{\rm bar} = 4n_0$ and thin ones, to $n_{\rm bar} = n_0$.

in the Boltzmann case at low temperatures the shear viscosity only weakly depends on the baryon density (cf. short-dashed curves in Fig.13). This has been noted earlier in [8]. Our results demonstrate important role played by the Pauli principle at low T and show a strong density dependence.

The model dependence of results is more pronounced for ζ. In the right panel of Fig.13 we present the partial contribution of the nucleon bulk viscosity for the multicomponent system. We see that in the SHMC model this contribution is very small and can be neglected. In the IG model the partial contribution, ζ_N, proves to be negative, whereas the total value ζ remains, certainly, positive.

The temperature dependence of the specific η/s and ζ/s transport coefficients is presented in Fig.14 for two values of the baryon density $1n_0$ and $4n_0$. The results of the SHMC (solid and dashed lines) and IG (dash-dotted and short-dashed lines) models differ not very much for the given value of the baryon density, except for the shear viscosity at low temperature due to the Pauli exclusion principle. The η/s for the baryon rich matter achieves the lower AdS/CFT bound $\eta/s = \frac{1}{4\pi}$ at smaller $T < T_c$ for the higher $n_{\rm bar}$.

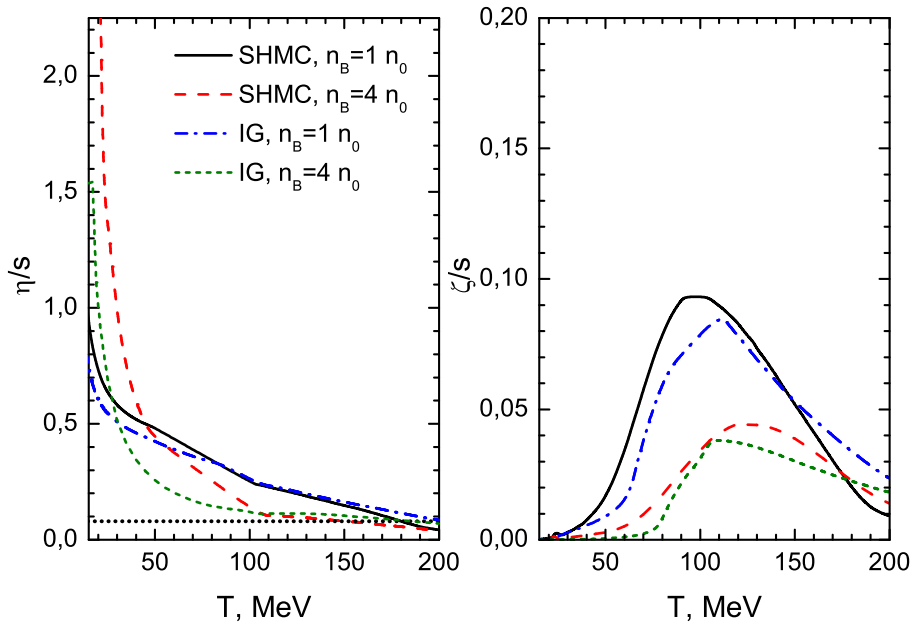

Fig. 14. The T-dependence of the specific viscosity coefficients η/s and ζ/s for two values of the baryon density $n_{\rm bar}$. Solid and dashed lines are our results for the SHMC model for n_0 and $4n_0$, respectively. The dash-dotted and dashed lines are calculations within the IG model with the same hadron set, again for n_0 and $4n_0$. Relaxation time is calculated following Eq. (58). The dotted line corresponds the the lower AdS/CFT bound $\eta/s = \frac{1}{4\pi}$.

5.4 Collisional viscosity in heavy ion collisions

Above we have studied the specific viscosities of the hadron matter at different temperatures and baryon densities. In reality a hot and dense system formed in a heavy-ion collision expands toward a freeze-out state, at which the components stop to interact with each other.

We should specially note that the approximations of the slow hydrodynamic expansion are violated at the freeze-out stage, which is assumed to be instantaneous within simple hydrodynamical models. More elaborated approach assuming continuous freeze-out decoupling demands some hybrid of kinetic and hydrodynamic description e.g., see [90,91]. Rapid processes out of equilibrium may lead to an additional dissipation and particle and entropy productions [88,89]. These effects are beyond the scope of the relaxation time approximation to the quasiparticle Boltzmann equation used in this work to evaluate the collisional viscosity. In addition, there are other sources contributing to viscosity, see e.g. Ref. [49] and also Appendix C. Here we use the phenomenological freeze-out curve $T_{\rm fr}(\mu^{\rm fr}_{\rm bar})$ extracted from the analysis of experimental particle ratios in statistical model for many species at the given collision en-

ergy $s_{NN}^{1/2}$ treating the freeze-out temperature $T_{\rm fr}$ and chemical potential $\mu_{\rm bar}^{\rm fr}$ as free parameters [86,87]. Thereby extra particle production is phenomenologically incorporated. We may also hope that including particle production effects we also partially include the corresponding effects of the entropy and viscosity productions.

In Fig. 15, η/s, ζ/s ratios are shown for Au + Au collisions versus the freeze-out temperature (which is unambiguously related to the freeze-out chemical potential $\mu_{\rm bar}^{\rm fr}$ [87] needed to calculate thermodynamical quantities at the freeze-out). As we see, the η/s ratio decreases monotonously with increase of the temperature, being higher than the lower bound $1/4\pi$ but tending to it with further increase of $T_{\rm fr}$. The value ζ/s exhibits a maximum at $T_{\rm fr} \sim 85$ MeV and then tends to zero with subsequent increase of $T_{\rm fr}$. As has been emphasized above, at $T \gtrsim 100$ MeV values of the shear and bulk viscosities become comparable in value, $(\eta/s)_{\rm fr} \simeq 2(\zeta/s)_{\rm fr}$.

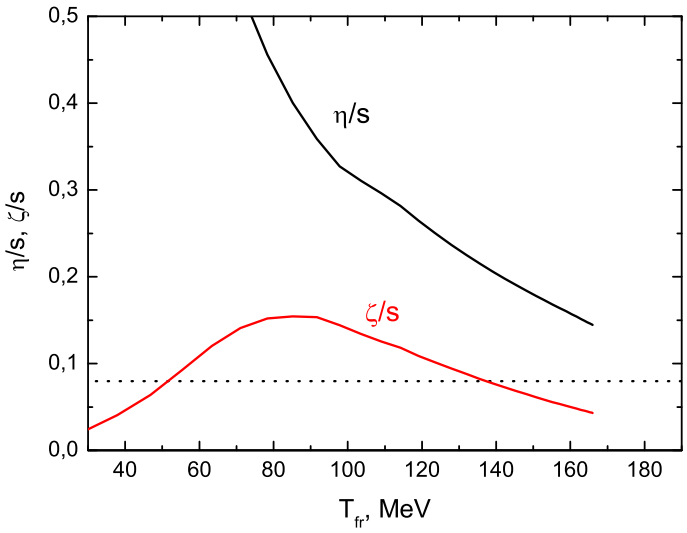

Fig. 15. Specific shear and bulk viscosities calculated in the SHMC model for central Au+Au collisions along the freeze-out curve (at $T = T_{\rm fr}$) [87] for the baryon enriched system. The dotted line is the lower AdS/CFT bound $\eta/s = 1/4\pi$ [31].

In Fig. 16, the η/s ratio calculated in our SHMC model (solid line) is plotted as a function of the collision energy $\sqrt{s_{NN}}$ of two Au+Au nuclei. The result for the IG model with the same hadron set as in SHMC model is plotted by the dash-dotted line. We note that for $\sqrt{s_{NN}} \gtrsim 3$ the SHMC results prove to be very close to the IG based model ones (with the same hadron set as in SHMC model), since the freeze-out density is rather small and the decrease of the hadron masses occurring in the SHMC model is not important. The results for the hadron hard core gas model (the van der Waals excluded volume model) [79] at two values of the particle hard core radius r are shown by dashed

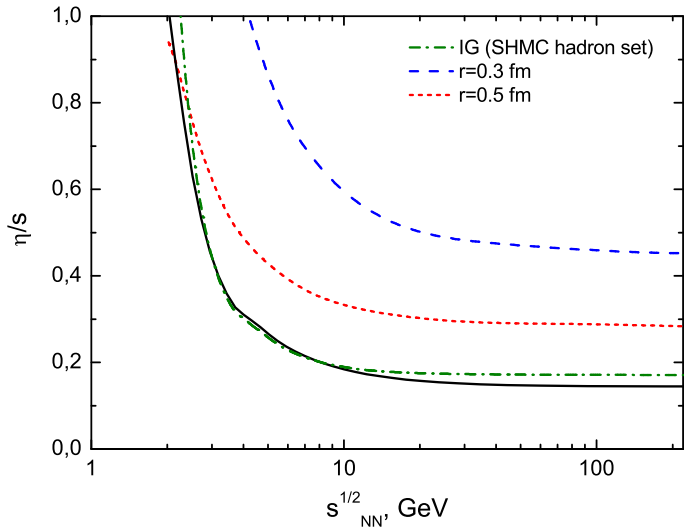

Fig. 16. The specific shear viscosity calculated for central Au+Au collisions along the chemical freeze-out curve [87] within the SHMC model as a function of the collision energy $s_{NN}^{1/2}$ (solid line). Dashed and short-dashed curves are the results of the excluded volume hadron gas model [79] with hard-core radii r =0.3 and r =0.5 fm, respectively. The dot-dashed line corresponds to the IG model with the same set of hadrons as for the SHMC model.

and short-dashed lines. In all cases for $\sqrt{s_{NN}} \gtrsim 2$ GeV the ratio η/s decreases along the chemical freeze-out line with increasing collision energy and then flattens at $\sqrt{s_{NN}} \gtrsim$10 GeV, since freeze-out at such high collision energies already occurs at almost constant value of $T_{\rm fr} \approx 165$ MeV. The shear viscosity of the non-relativistic Boltzmann gas of hard-core particles [79] is $\propto \sqrt{mT}/r^2$. Since Fermi statistical effects are not included within this model, the shear viscosity, η, decreases with decrease of T. Nevertheless the η/s ratio increases and diverges at low energy/temperature, as the consequence of a more sharp decrease of the entropy density compared to η, see Fig. 16. As follows from the figure, the smaller r is, the higher η/s is in the given excluded volume model. For $\sqrt{s_{NN}} \gtrsim 4$ and $r \simeq 0.7$ fm the η/s ratio is expected to be close to the values computed in the IG and SHMC models. We also note that in the whole range of the considered $\sqrt{s_{NN}}$ the SHMC results proved to be very close to the IG-based model expectation (with the same hadron set as in SHMC model) since the freeze-out density is small.

Recently an interesting attempt has been undertaken in [92] to extract the shear viscosity from the 3-fluid hydrodynamical analysis of the elliptic flow in the AGS-SPS energy range. An overestimation of experimental elliptic flow v_2 values obtained in this model was associated with dissipative effects occurring during the expansion and freeze-out stages of participant matter evolution. The resulting values of η/s vary in interval $\eta/s \sim 1-2$ in the considered domain of $\sqrt{s_{NN}} \approx 4-17$ GeV (corresponding to temperatures $T \approx 100-115$

MeV). Authors consider their result as an upper bound on the η/s ratio in the given energy range. Note that the mentioned values are much higher than those which follow from our estimations given above and presented in Figs. 15 and 16. One should additionally mention that the local equilibrium in the three-fluid models is established in every fluid but not among fluids in a common cell, whereas other models considered above imply a local thermal equilibrium.

Other microscopic estimate of the share viscosity to the entropy density ratio for the relativistic hadron gas based on the Kubo formulae was performed in Ref. [93]. Calculations were carried out by simulation of a system evolution in a box with appropriare boundary conditions using the UrQMD code, where 55 baryon species and their antiparticles and 32 meson species were included. The full kinetic and chemical equilibrium is achieved at T =130 and 160 MeV, respectively. Treating these temperatures as kinetic and chemical freeze-out ones and comparing them with those in Fig. 15, we see that the extracted ratio $\eta/s \gtrsim 1$ exceeds the SHMC result by a factor of 5. Introducing a non-unit fugacity or a finite baryon density allows one to decrease the ratio twice but nevertheless it is still too high as compared to both the SHMC result and the lower bound $\eta/s = 1/4\pi$. Analyzing their result authors [93] conclude that the dynamics of the evolution of a collision at RHIC is dominated by the deconfined phase (exhibiting very low values of η/s) rather than by the hadron phase. Note however that in-medium effects in the hadron phase are not included into consideration in the UrQMD model though, namely, these effects result in the required decrease of the η/s ratio in our SHMC model.

Similar dynamical estimate has been done recently in Ref. [94] where additionally to real hadrons the Hagedorn states were considered. Inclusion of heavy Hagedorn clusters decreases the η/s ratio at $T \lesssim 140$ MeV as compared to the UrQMD result [93] cited above but the obtained value $\eta/s \approx 0.3 - 0.4$ is still higher than the lower AdS/CFT bound and the Hagedorn gas statistical estimate for $\mu_{\rm bar}$ =0 [80] (see Fig. 8). It is worthy to note that for a finite chemical potential (or baryon density) the specific shear viscosity in [94] is getting lower but in contrast with our SHMC model (see Fig. 14) the lower AdS/CFT bound is not reached.

6 Shear and bulk viscosities in the quark phase

6.1 Estimates of the relaxation time

In the framework of the quasiparticle approximation the shear and bulk viscosities in the QGP phase can be found with the help of Eqs. (52), (53). These equations should be supplemented by expressions for the collisional relaxation time. Like in the hadron system, the collisional relaxation time τ_a, $a = \{q, g\}$, depends on the momentum. To simplify our calculations of the transport coefficients we will use for τ values $\tilde{\tau}_a$, where $\tilde{\tau}_a$ is estimated with the thermal averaged cross-sections describing total elastic scattering of medium constituents. Unlike the hadronic cross section the quark/gluon (parton) elastic scattering cross section is not measurable and should be evaluated in a model. Really, it is a specific problem. The in-medium cross sections for quark-antiquark, quark-quark and antiquark-antiquark scattering processes were studied in detail in Ref. [95] within the NJL model for two different flavors, including $1/N_c$ next-to-leading order corrections. These results incorporate dominance of the scattering on large angles and take into account a possible occupation of particles in the final state, see Ref. [96].

The QCD calculations of the relaxation time $\tilde{\tau}$ of partons already in the lowest order in the running coupling constant g require summation of infinitely many diagrams. Resummation of the hard thermal loops results in the width $\tilde{\tau}^{-1}$ of partons $\sim g^2 T \ln(1/g)$ [97]. Thus, the following parametrization was used for gluons [27,98]

$$\tilde{\tau}_g^{-1} = 2N_c \frac{g^2 T}{8\pi} \ln \frac{2c}{g^2}, \tag{60}$$

and similarly for quarks

$$\tilde{\tau}_q^{-1} = 2\frac{N_c^2 - 1}{2N_c} \frac{g^2 T}{8\pi} \ln \frac{2c}{g^2}, \tag{61}$$

where the running coupling constant is given by

$$g^2(T) = \frac{48\pi^2}{(11N_c - 2N_f) \ln(\lambda(T - T_s)/T_c)^2}\ , \tag{62}$$

which permits an enhancement near T_c (by construction, the hadron-quark phase transition in this model is of the first order). Parameters of the effective

coupling T_s and λ/T_c were adjusted to the lattice QCD EoS similar to what we did above for the two-phase EoS. One uses T_s/T_c =0.46 and the tuning parameter c is determined from the condition $g^2(T = T_c) = 0$ [27,99] that results in the divergence of the relaxation time at T_c (the cross section is zero at this point).

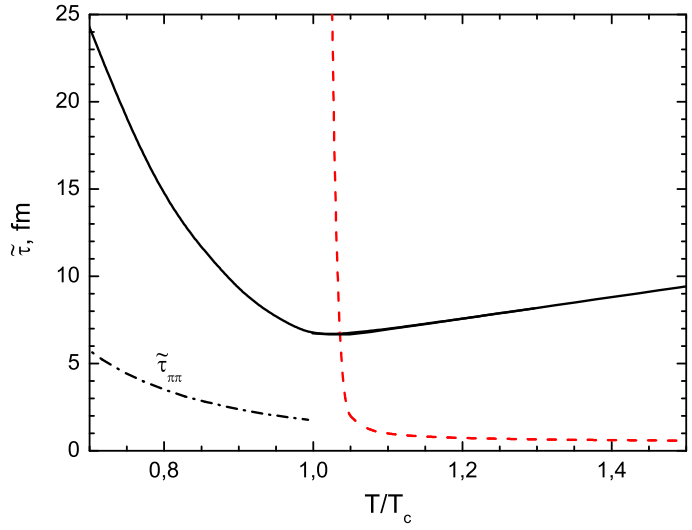

Fig. 17. Temperature dependence of the relaxation time $\widetilde{\tau}_q$ for $\mu_{\rm bar} = 0$. The solid line shows result of a calculation within the NJL model [96]. The quark relaxation time $\widetilde{\tau}_q$ estimated according to Eq. (61) at $T/T_c > 1$ is given by the dash line. For comparison the relaxation time $\widetilde{\tau}_{\pi\pi}$ obtained following Eq. (41), but only for the gas of massive free pions at $T/T_c < 1$, is plotted by the dash-dotted line.

The temperature dependence of $\tilde{\tau}_q$ for $\mu_{\rm bar} = 0$ within the NJL model [96] is shown in Fig. 17 by the solid line. Both $T < T_c$ and $T > T_c$ regions are covered in this model. However the NJL model, in which the medium is assumed to be composed only of heavy constituent quarks, can hardly be applied for the description of the $T < T_c$ phase. Therefore at $T < T_c$ for this phase we suggest to use the developed above hadronic description, where collisional time is calculated following Eq. (41) with experimental cross-sections for hadronic species. In the case $\mu_{\rm bar} = 0$ the main contribution is given by the pion term (see dash-dotted curve). In Fig. 17 we also show the relaxation time $\widetilde{\tau}_q$ for $T > T_c$ following (61), see the dashed line in figure. In order to obtain the relaxation time for gluons, $\widetilde{\tau}_g$, we should multiply $\widetilde{\tau}_q$ by the group factor 4/9.

6.2 Collisional viscosity in the quark-gluon phase

In the large N_c limit the specific shear viscosity in the QGP phase can be inferred from calculations of [35]

$$\left(\frac{\eta}{s}\right)_{QGP} = \left(\frac{1+3.974\xi}{1+1.75\xi}\right) \frac{69.2}{(g^2N_c)^2 \ln(26/(g^2N_c(1+0.5\xi))} \tag{63}$$

with $\xi = N_f/N_c$. Obviously this ratio in the quark/gluon phase at finite large N_c differs from that calculated for the hadronic phase. Therefore, one may expect a jump in the temperature dependence of the η/s-ratio at the crossing of the phase boundary of the first-order phase transition. In our HQB model

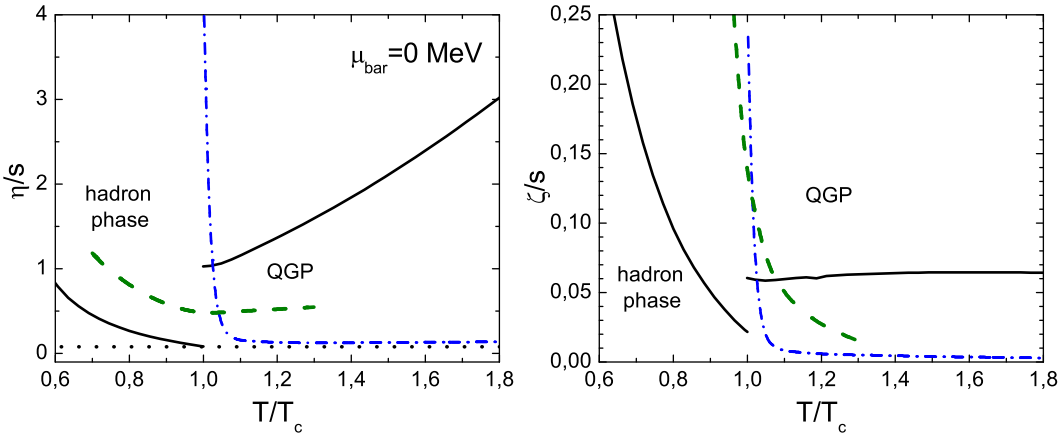

Fig. 18. The T-dependence of the shear (left panel) and bulk (right panel) specific viscosities within our two-phase SHMC-HQB model (solid lines) for $\mu_{\rm bar}$ =0. The results for the original NJL model [96] are plotted by dashed lines. The η/s and ζ/s calculated following Eqs. (52), (53) using quark masses from the HQB model and the relaxation time from (61) are shown by the dash-dotted lines. The lower bound for the reduced shear viscosity, $1/4\pi$, is given by the horizontal dotted line.

strange quarks and gluons are very massive. Therefore their contribution to transport coefficients and entropy density is minor. Main contributions arise from u- and d-quarks.

In Fig. 18, η/s and ζ/s for hadron and quark-gluon phases are shown in a broad temperature range for $\mu_{\rm bar} = 0$. Solid lines present results of the two-phase SHMC-HQB model. Below T_c the ratios are the same as shown above in Fig. 8. Calculations done in the NJL model [96] are shown by dashed lines. In both cases the quark collision relaxation time is that shown in Fig. 17 by the solid line. We see that the original NJL model [96] gives a continuous smooth line (a crossover) for $\mu_{\rm bar} = 0$. In our SHMC-HQB model there is a jump at T_c in both the η/s and ζ/s ratios. This jump is a particular property of the first order phase transition. For $\mu_{\rm bar}$ =0 in our two-phase SHMC-HQB model the η/s ratio increases with T more sharply after the jump has occurred compared to that in the original NJL model (see Fig. 18).

Dash-dotted curves in Fig. 18 demonstrate that the specific viscosities diverge for $T \to T_c + 0$ since $\widetilde{\tau} \to \infty$ provided the nonperturbative estimate of the

relaxation time (61) is used. With increase of the temperature above T_c the temperature dependence of these ratios flattens. The gluon η/s and ζ/s ratios exhibit in this case a similar divergent behavior near T_c, since the relaxation time (60) also diverges at $T_c + 0$. As follows from Eq. (63), in the QGP phase $\eta/s \propto 1/g^4$ where in accordance with (62) the coupling constant is expressed via $g^2 \propto 1/\ln(T/\Lambda_T)$, Λ_T is proportional to the scale parameter of QCD. Similar minimum close to T_c from the QGP side arises for the η/s for the gluon quasi-particle excitations in a phenomenological quasiparticle model [100] in agreement with lattice QCD data in gluodynamics [39,40,41]. Thus we conclude that both the magnitude of the jump and the η/s behavior for $T > T_c$ are essentially model-dependent. Generally, similar conclusion can be done from comparison of different curves for ζ/s in the right panel of Fig. 18.

Note that for the hadron phase the NJL model noticeably overshoots the SHMC model results for both η/s and ζ/s specific viscosities. However one should be careful comparing the NJL and SHMC-HQB results. The NJL model treats the chiral phase transition while in the SHMC-HQB model we deal with deconfinement. Thus, critical temperatures have different meaning in these models. Their values are also different (but the latter problem can be avoided provided one uses T/T_c as an argument). Moreover in the NJL model one continues to deal only with u and d quark degrees of freedom at $T < T_c$, whereas the SHMC model involves many hadron degrees of freedom whose masses essentially decrease at $T \sim T_c$. Thereby, the entropy density in the SHMC model is essentially higher and the specific viscosity is accordingly lower than those in the NJL model [96]. The shear viscosity-to-entropy ratio in the latter model is much higher than its lower bound $1/4\pi$ at $T \approx T_c$.

One should note that in our model the deconfined partonic phase is described in a simplified way as an ideal massive gas but relaxation times were taken from the models including interaction. A consistent approach requires an account for interactions between the constituents and the extracted effective couplings should enter the estimate for the transport cross section. A step toward this direction was undertaken in Ref. [101] within the generalized classical virial expansion formalism. The corrections to a single particle partition function were calculated starting from a parton interaction potential whose parameters are fixed by lattice thermodynamical quantities. The dependence of the η/s ratio on the temperature dependence of the strong interaction coupling has been studied. Results prove to be sensitive to the choice of the interaction.

There exist many other model estimates of the η/s ratio for $T > T_c$ for $\mu_{\rm bar} = 0$. As noted in the Introduction, AdS/CFT [21] predicts $\eta/s = 1/(4\pi)$. Lattice Monte Carlo calculations are available only for gluodynamics. For the SU(3) gauge theory a robust upper bound $\eta/s < 1$ was obtained with the best es-

timate $\eta/s = 0.134$ at $T = 1.65T_c$ [41]. A slightly larger value of the shear viscosity was derived in the lattice QCD simulation in the quench approximation for a hot gluon gas [39]: $\eta/s \simeq 0.1 \div 0.4$ for temperature in the region $1.4 \leq T_c \leq 1.8$. At higher temperatures η increases by two-three orders of magnitude.

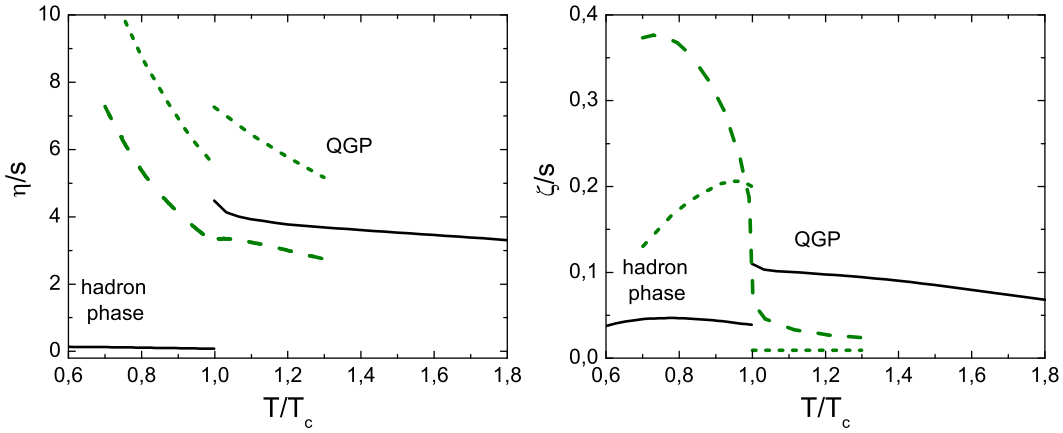

Fig. 19. The T-dependence of the shear (left panel) and bulk (right panel) specific viscosities within our two-phase SHMC-HQB model (solid lines) for $\mu_{\rm bar}^{\rm CEP}$ =990 MeV, corresponding to the critical end point. The NJL model results [96] for $\mu_{\rm bar}^{\rm CEP}$ and for $\mu_{\rm bar}$ slightly above $\mu_{\rm bar}^{\rm CEP}$ are plotted by long-dash and short-dash lines, respectively.

Model predictions for the η/s and ζ/s ratios for systems with $\mu_{\rm bar} \neq 0$ are presented in Fig.19. The NJL model [96] at the critical end point ($\mu_{\rm bar}$ =990 MeV) shows a smooth curve (long-dash line) with a sharp bend at T_c for η/s and ζ/s. Certainly, our two-phase model again exhibits a jump at T_c (see solid lines). Similar jump will appear in the NJL model if $\mu_{\rm bar}$ is larger than 990 MeV, *i.e.* when the system reaches the region of the first order phase transition (see short-dashed lines).

Here the following remark is in order: As follows from all above estimates, the bulk viscosity is smaller (but not much smaller in the hadron phase at finite baryon density) than the shear one in the whole temperature interval, may be except the vicinity of the critical point. In the latter region soft modes may additionally contribute significantly increasing the bulk viscosity.

In spite of a variety of existing models, none of them is reliable for the description of the vicinity of the critical point. In this respect, it is highly desirable to get experimental information about viscosity realized in heavy ion collisions to compare it with the model predictions. The shear viscosity is intimately related to the observed elliptic flow v_2 and viscous hydrodynamics provides a tool to extract η/s from experimental data. However, calculation uncertainties are significantly affected by details of the initialization of the

initial hydrodynamic state, behavior of the bulk viscosity and the speed of sound near the quark-hadron phase transition point, chemical composition and strong non-equilibrium effects during the late kinetic stage of the evolution of the hadronic state. From the study of transverse momentum fluctuations at the RHIC energies one gets $\eta/s \simeq 0.08 \div 0.3$ in Ref. [102]. Close estimates $\eta/s \simeq 0.08 \div 0.3$ and $\eta/s \simeq 0.09 \div 0.15$ were obtained from v_2 analysis in Refs. [103] and [104], respectively. In its turn, studies of the heavy quark energy loss and ϕ meson production yield $\eta/s \simeq 0.1 \div 0.16$ [105] and $\eta/s \simeq 0.07 \pm 0.003 \pm 0.014$ [106], respectively. Recent comprehensive analysis of the hydrodynamic simulations [107] has established an upper limit

$$\frac{\eta}{s}\Big|_{\rm QGP} < 5 \times \frac{1}{4\pi} \quad , \tag{64}$$

to be rather close to the low AdS/CFT bound. Note that the presence of $\zeta \neq 0$ can also result in a suppression of the elliptic flow v_2 competing at T near T_c with shear viscous effects [108]. Thus, the above constraint on η/s can be even stronger.

Finally, one should emphasize that practically in all viscous hydrodynamic calculations the specific ratio η/s is considered as a time-independent quantity, that is not the case, as follows from the above-presented dependence of kinetic coefficients on temperature and baryon density. In addition, it is tacitly neglected by retardation effects in the formation of irreversible current. Some exceptions are estimates [109,110]. In Ref. [109] viscosity effects were studied with two different T-dependent shear and bulk viscosities (treated as free parameters) in the QGP and hadronic phases. The values of the used transport coefficients noticeably differ from those presented in Figs.18 and 19. Following [109] the elliptic flow coefficient is significantly reduced due to viscosity effects both in the plasma and in the hadron matter. A more realistic parameterization of the temperature dependence of shear and bulk viscosity coefficients was considered in Ref. [110] and additionally relaxation times were included in order to explain elliptic flow at RHIC. It was argued that close to ideal behavior observed at RHIC energies may be related to a non-trivial temperature dependence of these transport coefficients. So, extraction of the shear viscosity from analysis of the initial QGP phase is a difficult problem which can be reliably addressed only after precise constraining the freeze-out conditions. Thus, at present there exist many different estimates of viscosity coefficients, being not consistent with each other and only indirectly related to the observed flow effects. Thus no definite conclusion can yet be done about temperature and density dependence of the transport coefficients in the QGP and hadron phases.

7 Beyond quasiparticle approximation

7.1 Generalization to finite particle mass-widths

Expressions (48), (49) for the shear and bulk viscosities were derived within the quasiparticle approximation, *i.e.*, the particle mass-width $\Gamma = -2\mathrm{Im}\Sigma^R$ was put zero in the retarded Green function G^R. Here Σ^R is the retarded self-energy. The spectral density ($\widehat{A} = -2\mathrm{Im}\widehat{G}^R$) is then expressed through the δ-function.

Let us start with the consideration of a fermion spin 1/2 resonance, "f". The spectral function satisfies the sum rule:

$$\frac{1}{4}\mathrm{Tr}\int_0^\infty \gamma_0 \left[\widehat{A}^{\mathrm{f}}_{(+)}(p_0,\vec{p}) + \widehat{A}^{\mathrm{f}}_{(-)}(p_0,-\vec{p})\right]\frac{dp_0}{2\pi} = 2, \tag{65}$$

where γ_0 is the corresponding Dirac matrix, and subscripts $(\pm)$ specify particle and antiparticle terms. The trace is taken over spin degrees of freedom. Simplifying the spin structure we introduce the spectral density

$$A^{\mathrm{f}} = \frac{1}{4}\mathrm{Tr}\{\ \gamma_0\widehat{A}^{\mathrm{f}}_{(+)}\}. \tag{66}$$

Consider the dilute matter assuming that the spectral function depends only on the variable $s = p_0^2 - \vec{p}^{\,2} > 0$, see [111]. To do the problem tractable, instead of solving a complete set of the Dyson equations, we will use a simplified phenomenological expression [58]:

$$A^{\mathrm{f}} = \bar{A}^{\mathrm{f}} 2p_0 = \frac{\xi\ 2p_0\ [\bar{\Gamma}^{\mathrm{f}}(s)+\delta]}{(s - m_{\mathrm{f}}^{\mathrm{part}*2})^2 + [\bar{\Gamma}^{\mathrm{f}}(s)+\delta]^2/4}, \quad \xi = const, \tag{67}$$

with $\delta \to +0$ introduced to easier perform the quasiparticle limit. The value $\bar{\Gamma}^{\mathrm{f}}(s)$ is the width. Phenomenological expression for its s-dependence is presented in Appendix B.

For charged bosons the spectral function has the form: [6]

[6] As before, by the charge we mean any conserved quantity like electric charge, strangeness, etc.

$$A_{\rm bos} = \frac{\xi\ [\Gamma_{\rm bos}(s) + \delta]}{(s - (m_{\rm bos}^{\rm part*})^2)^2 + [\Gamma_{\rm bos}(s) + \delta]^2/4}. \tag{68}$$

Replacing $\Gamma_{\rm bos}(s)$ with $\bar{\Gamma}(s)$ and $A_{\rm bos}$ with $\bar{A}$, we may use Eq. (82) of Appendix B as a phenomenological parameterization of the width. The quantity ξ is introduced to fulfill the sum-rule in the form

$$\int_0^\infty ds \frac{\bar{A}_{\rm f}^2(s)\bar{\Gamma}_{\rm f}(s)}{2} = \int_0^\infty ds \frac{A_{\rm bos}^2(s)\Gamma_{\rm bos}(s)}{2} = 1. \tag{69}$$

We continue to study dilute matter assuming that the spectral function depends only on the s-variable. Only in this case one may consider a single spectral function for vector mesons, like ω and ρ, whereas in the general case one should introduce transversal and longitudinal components. Now we conjecture expression for the shear viscosity which generalizes quasiparticle expression obtained above to the case of the finite mass-width

$$\eta = \frac{1}{15T}\sum_a \int g_a \frac{d^3p_a}{(2\pi)^4} \int_0^\infty ds \frac{\bar{A}_a^2(s)\bar{\Gamma}_a(s)}{2}\, \tau_a \frac{\vec{p}_a^{\,4}}{E_a^2}\, F_a^{\rm eq}(p_0)(1 \pm F_a^{\rm eq}(p_0)). \tag{70}$$

Here we have put $\tau_a = 2p_0/\bar{\Gamma}_a(s)$, $E_a = \sqrt{(m_a^{\rm part*})^2 + \vec{p}^2}$,

$$F_a^{\rm eq}(p_0) = \frac{1}{e^{(p_0 - \mu_a^*)/T} \pm 1}. \tag{71}$$

Derivation of this expression will be given elsewhere. In the nonrelativistic approximation Eq. (70) coincides with the corresponding expression derived in [112].

In the quasiparticle approximation

$$\frac{\bar{A}_{\rm f}^2\bar{\Gamma}_{\rm f}}{2} \to 2\pi\delta(s - (m_{\rm f}^{\rm part*})^2), \quad \frac{A_{\rm bos}^2\Gamma_{\rm bos}}{2} \to 2\pi\delta(s - (m_{\rm bos}^{\rm part*})^2), \tag{72}$$

and we return to Eqs. (48) – (49) with $\tau_a = 2E_a/\bar{\Gamma}_a(E_a)$. Here the relaxation time for the a-quasiparticle is expressed through the width, rather than the cross-section. Bearing in mind the optical theorem, these two quantities should coincide within the quasiparticle approximation. This statement however requires an additional check that we do not perform in the given work, since our aim here is just to estimate possible effects of finite widths on the viscosities. Moreover in the case of a finite width the off-mass shell $\tau_a(p_0, \vec{p})$ enter our expressions.

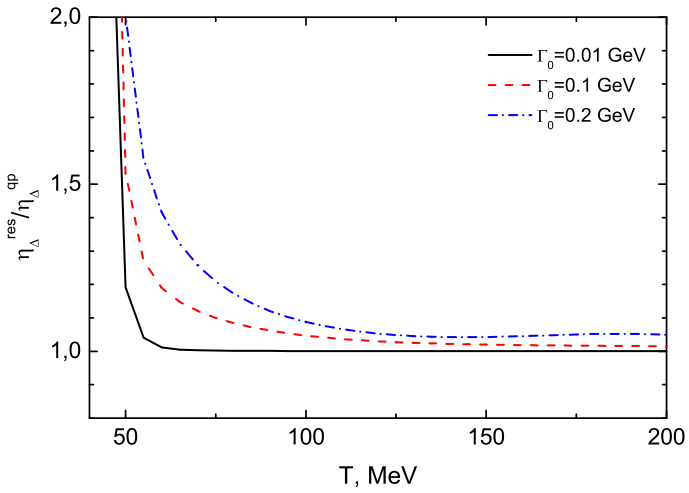

Fig. 20. Temperature dependence of the ratio of the shear viscosity for the resonance calculated in the constant width approximation at different values of $\bar{\Gamma} = \Gamma_0 m_{\rm res}$ to that computed in the quasiparticle approximation. In both (resonance and quasiparticle) cases we use the same (for the given Γ_0) energy-momentum independent values of the relaxation times and $m_{\rm res} = m_\Delta$. Lines show different values of the width.

In Fig. 20, we show the temperature dependence of the ratio of the shear viscosity calculated for the resonance ($m_{\rm res} = m_\Delta$ =1.232 GeV) in the constant width approximation ($\Gamma = \Gamma_0 m_{\rm res}$) with the constant relaxation time to that computed in the quasiparticle approximation with the same relaxation time. Realistic value of the Δ-resonance width in the resonance maximum is $\Gamma^{\rm n.rel.} \simeq 120$ MeV that corresponds to the choice $\Gamma_0 = 0.24$ GeV. In order to understand the dependence of the shear viscosity on the value of the width we vary the value Γ_0. We see that width effects are quite important for the description of the resonance characteristics at low temperatures $T \lesssim 50 \div 100$ MeV, whereas at higher temperatures one may use quasiparticle approximation. At low temperatures contribution of the resonances to the transport coefficients and to the thermodynamical quantities is suppressed compared to the nucleon and pion contributions. However, since even for very small width (for $\Gamma_0 = 0.01$ GeV corresponding to $\Gamma^{\rm n.rel.} \sim 5$ MeV) the quasiparticle approximation for calculation of the viscosity fails for $T < 50$ MeV, and since nucleons have some width, we may conclude that calculations of the transport coefficients at low temperatures should be performed with taking into account width effects.

It was argued in [113] that in a theory, where the lowest energy excitations (not quasiparticles) form a continuum, the η/s ratio has no lower bound in contrast with predictions of the AdS/CFT correspondence. To check this statement we calculated η/s ratios. For the free resonance gas the entropy density is given by [111,114],

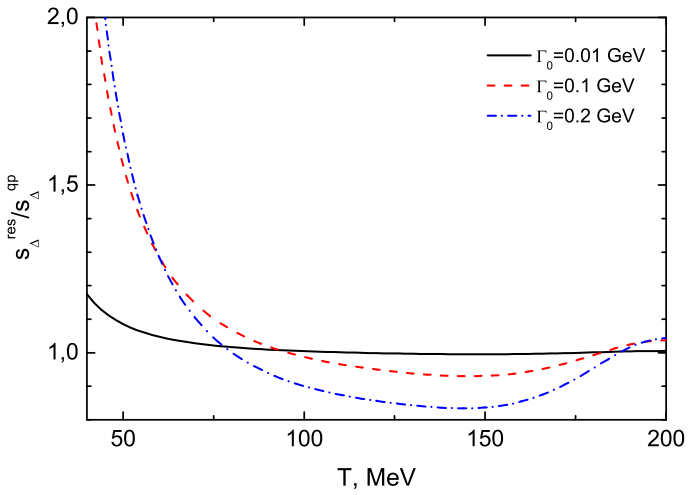

Fig. 21. Temperature dependence of the ratio of the entropy densities for the resonance calculated with constant width and in the quasiparticle approximation, $m_{\rm res} = m_\Delta$. The curves are drown for different values of the width.

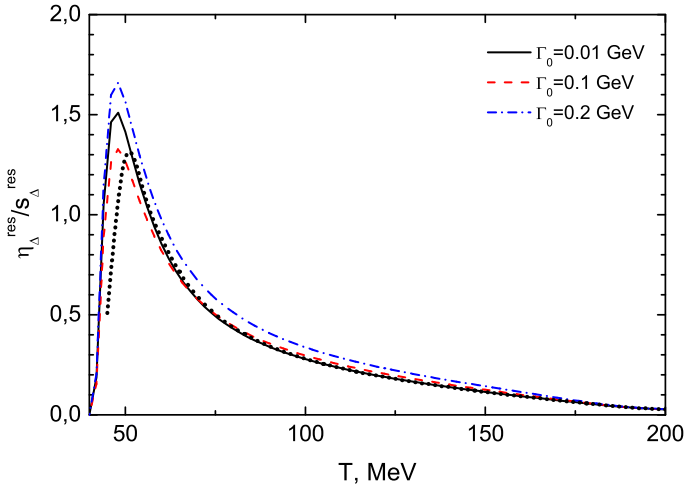

Fig. 22. Temperature dependence of the specific shear viscosity for the Δ resonance calculated in the constant width approximation, $m_{\rm res} = m_\Delta$. The quasiparticle result is plotted by dots.

$$s_{\rm f} = \sum_a g_a \int \frac{d^3p}{(2\pi)^4} \int_0^\infty ds \bar{A}_a \sigma_a \tag{73}$$

where $\sigma_a = \mp(1 \mp F_a^{\rm eq}) \ln(1 \mp F_a^{\rm eq}) - F_a^{\rm eq} \ln F_a^{\rm eq}$ and $F_a^{\rm eq}$ is determined by Eq. (71).

In Fig. 21 we present the ratio of the entropy density computed with taking into account width effects to that calculated in the quasiparticle approximation. As for the viscosity, in case of small width (see solid curve for $\Gamma_0 = 0.01$ GeV) the ratio $s^{\rm res}/s^{\rm qp}$ deviates from unity only for low temperatures (at

$T < 50$ MeV). For a larger width the ratio begins to significantly differ from the unity in the whole temperature interval.

In Fig. 22 the temperature dependence of the $\eta^{\rm res}/s^{\rm res}$ ratio is shown for $m_{\rm res} = m_\Delta$ and for different values of Γ_0. We see that the dependence on the value of the width is rather moderate. The ratio calculated in the quasiparticle approximation behaves in a similar way but the maximum position is slightly shifted toward a higher temperature. For large temperatures the quasiparticle limit is achieved and, thereby, within our model the η/s ratio reaches the limit $1/4\pi$ at $T \simeq T_c \sim 180$ MeV.

7.2 Mean-field bulk viscosity term

The sources of the shear and bulk viscosities considered above are associated with collisions between in-medium excitations (quasiparticles and particles with widths). Another source of the bulk viscosity may come from a dissipation of the soft modes related to a slow dynamics of the mean fields provided the system is located in the vicinity of the critical point of a second order phase transition or at a weak first order phase transition. Note that in our SHMC model the soft modes relate to the hadron masses decreasing towards the critical point T_c. Such a contribution was first introduced in [47,48] and then discussed in [49,50,51]. Within the quasiparticle approximation used above, the mean fields do not dissipate. Thereby, there are no linear in ∂_μ terms in (43) responsible for an additional bulk viscosity term. In reality there may exist such a dissipation. We demonstrate possible effect of a dissipation on the bulk viscosity in Appendix C. However we should note that considering the soft mode viscosity regime one assumes that the time characterizing the soft mode evolution is sufficiently long. Estimations [54] show that soft modes may not develop during the time, at which the system trajectory in the course of the heavy ion collision passes the vicinity of the critical point. Thus the particle collisions look a more adequate source of the viscosity in heavy ion collisions than a source due to the soft mode evolution. Therefore in the given paper we focused on discussion of the collisional source for the viscosities.

8 Conclusions

In this paper, we analyzed different approximations for the calculation of the shear and the bulk viscosities for the hadron and the quark-gluon phases. General expressions for shear and bulk viscosities are derived in the relaxation-time approximation for a system described by the quasipartcle relativistic

mean-field theory with the scaling of hadron masses and couplings (SHMC). The EoS of the SHMC model fairly well reproduces global properties of hot and dense hadron matter including the temperature region near T_c and the lattice data for $T_c \lesssim T \lesssim 1.3T_c$, provided all coupling constants $g_{\sigma b}$ are strongly suppressed except for the nucleons.

We compared kinetic coefficients calculated in the SHMC model with those calculated in other models of the hadron phase. At $\mu_{\rm bar} = 0$ a general fall off of the specific shear viscosity with temperature in hadronic phase is a common feature for all models but quantitative values are somewhat different particularly showing different behavior in the temperature region near the transition temperature T_c. The η/s ratio in the SHMC model is closer to that of the excluded volume hadron-resonance gas model with the hard-core radius $r \simeq 0.7$ fm [79] and practically coincides in the near-critical region with a resonance gas model result that includes Hagedorn states [115].

For $\mu_{\rm bar} \neq 0$ transport coefficients qualitatively behave similarly to the case of baryonless matter reaching the lower AdS/CFT bound for the specific shear viscosity $\eta/s = 1/4\pi$ with increase of T. For the higher baryon density this limit is reached at smaller T. In particular, with increasing freeze-out temperature $T_{\rm fr}$ (for central Au+Au collisions), the η/s ratio undergoes a monotonous decrease approaching values close to the AdS/CFT bound at $T \sim T_c$,[7] while the ζ/s ratio exhibits a maximum at $T_{\rm fr}$ ∼85 MeV. In a broad temperature interval the η/s and ζ/s ratios are not small and viscous effects can be noticeable. The viscosity values at the freeze-out can be transformed into dependence on the colliding energy $\sqrt{s_{NN}}$ (for central Au+Au collisions). When the collision energy decreases, the η/s goes up. The high-energy flattening of the $\sqrt{s_{NN}}$ dependence occurs at quite low $\eta/s < 0.2$. It implies that a small value of η/s required for explaining a large elliptic flow observed at RHIC could be reached in the hadronic phase. This might be an important observation which we have demonstrated within the SHMC and the ideal gas (IG) models with the same hadron set. The η/s and ζ/s ratios at the freeze-out curve calculated within the SHMC and IG models agree with each other; however, rough estimates [92,93,94] of η/s extracted from comparison of dynamical model calculations with experimental data overshoot these theoretical expectations by a factor of 2-5. Note that rapid processes at the freeze out may result in an additional increase of the viscosities and the entropy production. These effects are not incorporated directly in the present consideration but the use of experimental freeze-out temperature and chemical potential allows one to hope that indirectly they are effectively included.

[7] We remind that there exist rather general arguments that η/s should have a minimum at the QCD phase transition critical point similar to that exists for helium, nitrogen and water, see [37].

Using the Gibbs conditions we extended our approach to higher temperatures combining the SHMC model description of the hadron phase with that of the heavy quark bag (HQB) model for the quark-gluon phase. It was demonstrated that this two-phase SHMC-HQB model is in reasonable agreement with QCD lattice data at $\mu_{\rm bar}$ =0 and $\mu_{\rm bar} \neq$0 at all temperatures except a vicinity of the critical point. The finite-size and nonequilibrium effects of the phase mixture, possibility of a rapid phase transition without a phase mixture may lead to significant additional dissipation provided the system trajectory passes the vicinity of the critical point. Moreover one might be need to improve the model in order to include possibility of the crossover for $\mu_{\rm bar} = 0$. Not considered in our work these effects require a special careful analysis.

In the two-phase SHMC-HQB model with the first order phase transition there appears a jump in both η/s and ζ/s at the critical temperature at any $\mu_{\rm bar}$. For $T > T_c$ at $\mu_{\rm bar} = 0$, η/s grows with increase of the temperature, whereas ζ/s approximately stays constant. The magnitude of both ratios differs significantly from those estimated in the NJL model [59,96]. Comparison of our approach with the NJL model [59,96] demonstrates that behavior of transport coefficients near the critical point depends on the type of the phase transition.

It is worthy to note that the v_2 analysis [116] indicates different values of η/s for peripheral and central collisions. Therefore, it would be interesting to perform hydrodynamical calculations using the $T - \mu_{\rm bar}$ dependent transport coefficients rather than constant ones. Necessity of such an approach was recently emphasized in [116]. In subsequent works we plan to use the SHMC model EoS with the derived transport coefficients for this purpose.

We also estimated influence of the finite width effects on the transport coefficients. For this aim we evaluated the shear viscosity and the entropy density at non-zero width. Our findings show that width effects are important for low temperatures (for $T \lesssim (50 \div 100)$ MeV), whereas for higher temperatures one may use the quasiparticle approximation.

As was demonstrated in [50,51] the ζ/s ratio may have a sharp maximum at the critical point. This statement is based on the assumption of the existence of soft collective modes at temperatures near T_c. The enhancement of the ratio ζ/s near the critical point could have interesting consequences [15,17,43,45,117], provided the system evolves very slowly. However it is unlikely that in the course of relativistic heavy ion collisions the system spends enough time in the vicinity of the critical point to develop slow soft collective modes, see [54,118]. Moreover effective hadron masses responsible for the softness of the modes, being calculated within our SHMC model, although decrease toward the critical point do not drop to zero. Thus the quasiparticle-like collisional viscosity estimates look more relevant than those follow from the considera-

tion of the slow soft mode dynamics. One should remind once more that other sources for an increase in the bulk viscosity may exist, as discussed in [49]. Therefore further studies of the given problem are still required.

Acknowledgements

We are grateful to K.K. Gudima, Y.B. Ivanov, Y.L. Kalinovsky, E.E. Kolomeitsev, K. Redlich and V.V. Skokov for numerous discussions and valuable remarks. We are thankful to K. Redlich for providing tables for values of the relaxation time calculated within the NJL model. This work was supported in part by the the DFG grants 436 RUS 113/558/0-3 and WA 431/8-1, Ukrainian-RFBR grant N 09-02-90423-Ukr-f-a and the Heisenberg-Landau grant.

Appendix A. Necessary formulas for derivation of transport coefficients.

Here to take derivatives in (42) we follow the line of Refs. [45,59]. The only difference is that the strangeness conservation is additionally incorporated.

The energy density ϵ and the baryon and strangeness charge density ($n_{\rm bar}$ and $n_{\rm str}$) conservations can be expressed as

$$\frac{\partial \epsilon}{\partial t} = -(\epsilon + P)\vec{\nabla}\cdot\vec{u} = -\left(T\frac{\partial P}{\partial T} + \mu_{\rm bar}\frac{\partial P}{\partial \mu_{\rm bar}} + \mu_{\rm str}\frac{\partial P}{\partial \mu_{\rm str}}\right)\vec{\nabla}\cdot\vec{u}, \quad (74)$$

$$\frac{\partial n_{\rm bar}}{\partial t} = -n_{\rm bar}\vec{\nabla}\cdot\vec{u} = -\frac{\partial P}{\partial \mu_{\rm bar}}\vec{\nabla}\cdot\vec{u}, \quad (75)$$

$$\frac{\partial n_{\rm str}}{\partial t} = -n_{\rm str}\vec{\nabla}\cdot\vec{u} = -\frac{\partial P}{\partial \mu_{\rm str}}\vec{\nabla}\cdot\vec{u}\ . \quad (76)$$

Here we set $\vec{u} = 0$ keeping only derivative terms of $\vec{u}$. The pressure is expressed in terms of T, μ variables. Further expressing P in terms of ϵ, n variables and using Eqs. (74)–(76) we find

$$\begin{aligned}\frac{\partial P[\epsilon,n]}{\partial t} &= \frac{\partial P}{\partial \epsilon}\frac{\partial \epsilon}{\partial t} + \frac{\partial P}{\partial n_{\rm bar}}\frac{\partial n_{\rm bar}}{\partial t} + \frac{\partial P}{\partial n_{\rm str}}\frac{\partial n_{\rm str}}{\partial t} \\ &= -\left[\frac{\partial P}{\partial \epsilon}\left(T\frac{\partial P}{\partial T} + \mu_{\rm bar}\frac{\partial P}{\partial \mu_{\rm bar}} + \mu_{\rm str}\frac{\partial P}{\partial \mu_{\rm str}}\right)\right. \\ &\quad \left. + \frac{\partial P}{\partial n_{\rm bar}}\frac{\partial P}{\partial \mu_{\rm bar}} + \frac{\partial P}{\partial n_{\rm str}}\frac{\partial P}{\partial \mu_{\rm str}}\right]\vec{\nabla}\cdot\vec{u}. \end{aligned} \quad (77)$$

On the other hand

$$\frac{\partial P[T,\mu]}{\partial t} = \frac{\partial P}{\partial T}\frac{\partial T}{\partial t} + \frac{\partial P}{\partial \mu_{\rm bar}}\frac{\partial \mu_{\rm bar}}{\partial t} + \frac{\partial P}{\partial \mu_{\rm str}}\frac{\partial \mu_{\rm str}}{\partial t} \tag{78}$$

and thus

$$\frac{\partial T}{\partial t} = -T\left(\frac{\partial P}{\partial \epsilon}\right)_{n_{\rm bar},n_{\rm str}} \vec{\nabla}\cdot\vec{u}, \tag{79}$$

$$\frac{\partial \mu_{\rm bar}}{\partial t} = -\left[\mu_{\rm bar}\left(\frac{\partial P}{\partial \epsilon}\right)_{n_{\rm bar},n_{\rm str}} + \left(\frac{\partial P}{\partial n_{\rm bar}}\right)_{\epsilon,n_{\rm str}}\right]\vec{\nabla}\cdot\vec{u}, \tag{80}$$

$$\frac{\partial \mu_{\rm str}}{\partial t} = -\left[\mu_{\rm str}\left(\frac{\partial P}{\partial \epsilon}\right)_{n_{\rm bar},n_{\rm str}} + \left(\frac{\partial P}{\partial n_{\rm str}}\right)_{\epsilon,n_{\rm bar}}\right]\vec{\nabla}\cdot\vec{u}. \tag{81}$$

We use these equations to construct variation of the energy-momentum tensor δT^{ij} in Eq. (45).

Appendix B. Phenomenological expression for the width of the resonance.

The phenomenological expression for the s-dependence of the width $\bar{\Gamma}^{\rm f}(s)$ can be easily recovered in the near threshold region, see [58],

$$\bar{\Gamma}^{\rm f}(s) = \Gamma_0\ F(s)\ m^{\rm f}\left(\frac{s^{1/2}-s_{\rm th}^{1/2}}{m^{\rm f}-s_{\rm th}^{1/2}}\right)^{\alpha}\theta(s-s_{\rm th})\ , \tag{82}$$

$$F = \frac{1}{1+[(s-s_{th})/s_0]^{\beta}}.$$

Here $\alpha = 1/2$ for the s-wave resonance and $3/2$ for the p-wave resonance, $m^{\rm f}$ is the fermion resonance mass in vacuum, and $s_{\rm th}$ is the threshold value of s; Γ_0 is the constant of the dimensionality of the energy. In order to use this expression outside the near threshold region one introduces the form-factor $F(s)$, the s_0 is the cut-off constant and the power $\beta > 1+\alpha/2$. The parameters can be adjusted to satisfy experimental data. The factor ξ is introduced to fulfill the sum-rule:

$$\int_0^\infty \frac{{\rm d}s}{2\pi}\bar{A}_{\rm f} = 1\ . \tag{83}$$

For charged bosons the spectral function follows the sum-rule,

$$\int_0^\infty \frac{ds}{2\pi}A_{\rm bos} = 1\ . \tag{84}$$

Appendix C. Contribution of soft collective modes to the bulk viscosity

As follows from the particle data, in vacuum the width of the σ meson is very large, $\Gamma_\sigma \sim 400$ MeV. In hot baryonic matter the width can additionally increase due to a collisional broadening. Supposing $\sigma = \sigma_{\rm eq} + \delta\sigma$ in the equation of motion for the mean field, where $\sigma_{\rm eq}$ is the equilibrium value of the mean field, we arrive at the equation for the fluctuating mean field part $\delta\sigma$:

$$(m_\sigma^{*\rm part}[T,\mu])^2 \delta\sigma = -\Gamma_\sigma \frac{\partial \delta\sigma}{\partial t}, \tag{85}$$

$1/\Gamma_\sigma$ is the relaxation time for the given process. We suppressed the second space-time derivative terms but included the first time-derivative dissipation term in this equation with a pre-factor Γ_σ. From Fig. 1 we see that for the zero baryon chemical potential in the SHMC model with suppressed couplings $g_{\sigma b}$, except for the nucleons, which we use in the given paper, the effective mass $m_\sigma^{*\rm part}$ significantly decreases at $T \sim T_c$.

Using smallness of the time-derivative term in (85) we find

$$\delta\sigma = -\frac{\Gamma_\sigma^{\rm eq}}{(m_\sigma^{*\rm part})^2_{\rm loc.eq}} \; \frac{d\sigma_{\rm loc.eq}}{dt}, \tag{86}$$

where $\sigma_{\rm loc.eq}$ is the mean field value at the local equilibrium. On the other hand,

$$\frac{d\sigma_{\rm loc.eq}}{dt} = \frac{d\sigma_{\rm loc.eq}}{ds} \; \frac{ds}{dt} = \frac{d\sigma_{\rm loc.eq}}{ds} \; s_{\rm loc.eq} \; \vec{\nabla}\cdot\vec{u}, \tag{87}$$

where we used approximate conservation of the entropy (up to terms proportional to transport coefficients assumed to be small). Since the bulk viscosity contribution of the mean field is related to the pressure as $\zeta_{\rm MF} \; \vec{\nabla}\cdot\vec{u} = -\delta P_{\rm MF}$, we find

$$\zeta_{\rm MF} = -\left(\frac{\partial P_{\rm MF}}{\partial\sigma}\right)_\epsilon \frac{\delta\sigma}{\vec{\nabla}\cdot\vec{u}} = \left(\frac{\partial P_{\rm MF}}{\partial\sigma}\right)_\epsilon \left[\frac{\Gamma}{(m_\sigma^{*\rm part})^2}\frac{d\sigma}{ds}s\right]_{\rm loc.eq}, \tag{88}$$

and $[\frac{d\sigma}{ds}]_{\rm loc.eq} = [\frac{d\sigma}{dT}/\frac{ds}{dT}]_{\rm loc.eq}$ is taken at the condition that equations of motion (11) are fulfilled.

There exist arguments that the ρ-meson also becomes a broad resonance at T near T_c, see [119], and its effective mass decreases with increase of T towards

T_c. The ρ-mean field appears in isotopically asymmetric nuclear matter. In this case, there may appear an extra contribution to the bulk viscosity. A similar contribution from the fluctuation of the ω_0 field is probably suppressed compared to that from the σ, since $\Gamma_\omega \ll \Gamma_\sigma$.

References

[1] S. Chapman and T. Couling, "The mathematical theory of non-uniform gases", Cambridge University Press, 1970.

[2] S.R. Elliott, "Physics of amorphous materials", Longman Group Ltd., London 1983.

[3] S. de Groot, W. van Leeuwen and Ch. van Weert, "Relativistic kinetic theory", North-Holland, Amsterdam, 1980.

[4] T. Schafer, Phys. Rev **A76**, 0636 (2007); T. Schafer and D. Teaney, Rept. Prog. Phys. **72**, 126001 (2009).

[5] G. Baym and C. Pethick, in "The physics of liquid and solid helium", Part II, ed. K. Benneman and I. Ketterson, Wiley, 1978.

[6] I.M. Khalatnikov, "Introduction in Theory of Superfluids", Moscow, Nauka, 1965 (in Russian).

[7] J.L. Anderson and H.R. Witting, Physica **74**, 466 (1973); Physica **74**, 489 (1973).

[8] V.M. Galitsky, Yu.B. Ivanov and V.A. Khangulian, Sov. J. Nucl. Phys. **30**, 401 (1979).

[9] P. Danielewicz, Phys. Lett. **B146**, 168 (1984).

[10] R. Hakim, L. Mornas, P. Peter, and H.D. Sivak, Phys. Rev. **D46**, 4603 (1992).

[11] R. Hakim and L. Mornas, Phys. Rev. **C47**, 2846 (1993).

[12] S. Weinberg, Astrophys. J. **168**, 175 (1971).

[13] T.A. Thompson, E. Quataert and A. Burrows, Astroph. J., **620**, 861 (2005).

[14] N. Auerbach and S. Shlomo, Phys. Rev. Lett. **103** 172501 (2009).

[15] P. Danielewicz and M. Gyulassy, Phys. Rev. **D31**, 53 (1985).

[16] S. Gavin, Nucl. Phys. **A435**, 826 (1985).

[17] A. Hosoya and K. Kajantie, Nucl. Phys. **B250**, 666 (1985); A. Hosoya, M.-A. Sakagami and M. Takao, Ann, Phys. **154**, 229 (1984).

[18] G. Baym, H. Monien, C.J. Pethick and D.G. Rosenhall, Phys. Rev. Lett. **64**, 1867 (1990).

[19] Huchao Song, arXiv: 0908.3656 [nucl-th].

[20] P. Arnold, G.D. Moore and L.G. Yaffe, JHEP **11** 001 (2000); JHEP **05**, 051 (2003).

[21] G. Policastro, D.T. Son and A.O. Starinets, Phys. Rev. Lett. **87**, 081601 (2001).

[22] G.D.Moore, JHEP **09105**, 039 (2001).

[23] M.A. Valle Basagoiti, Phys. Rev. **D66**, 045005 (2002).

[24] G. Aarts and J.M. Martínez Resco, JHEP **0211**, 022 (2002).

[25] A. Buchel, J.T. Liu and A.O. Starinets, Nucl. Phys. **B707**, 56 (2005).

[26] H. Defu, arXiv:hep-ph/0501284.

[27] A. Peshier and W. Cassing, Phys. Rev. Lett. **94**, 172301 (2005).

[28] S.S. Adler et al., (PHENIX Collaboration), Phys. Rev. Lett. **91**, 182301 (2003); J. Adams et al. (STAR Collaboration), Phys. Rev. Lett. **92**, 052302 (2004).

[29] D. Teaney, Phys. Rev. **C68**, 034913 (2005); P. Romatschke and U. Romatschke, Phys. Rev. Lett. **99**, 172301 (2007); M. Luzum and P. Romatschke, Phys. Rev. **C78**, 034915 (2008); K. Dusling and D. Teaney, Phys. Rev. **C77**, 034905 (2008); U.W. Heinz, Phys. Lett. **B658**, 279 (2008); H. Song and U.W. Heinz, Phys. Rev. **C77**, 064901 (2008); A.K. Chaudhuri, arXiv:0801.3180 [nucl-th].

[30] E.V. Shuryak, Nucl. Phys. **A750**, 64 (2005); M. Gyulassy and L. McLerran, Nucl. Phys. **A750**, 30 (2005); U.W. Heinz, arXiv:nucl-th/0512051.

[31] P. Kovtun, T.D. Son and O.A. Starinets, JHEP **0310**, 064 (2003); Phys. Rev. **94**, 111601 (2005).

[32] S.C. Huot, S.Jeon and G.D. Moore, Phys. Rev. Lett. **98**, 172303 (2007).

[33] S. Pu and Q. Wang, arXiv:0810.5271 [hep-ph].

[34] B.-C. Li and M. Huang, Phys. Rev. **D78**, 117503 (2008).

[35] J.I. Kapusta, arXiv:0809.3746 [nucl-th].

[36] E.V. Shuryak and I. Zahed, Phys. Rev. **C70**, 021901 (2004); Phys. Rev. **D69**, 046005 (2004).

[37] L.P. Csernai, J.I. Kapusta and L.D. McLerran, Phys. Rev. Lett. **97**, 152303 (2006).

[38] F. Karsch, E. Laermann and A. Peikert, Phys. Lett. **B478**, 447 (2000).

[39] A. Nakamura and S. Sakai, Phys. Rev. Lett. **94**, 072305 (2005); A. Nakamura and S. Sakai, Nucl. Phys. **A774**, 775 (2006).

[40] S. Sakai and A. Nakamura, PoS LAT 2007, 221 (2007).

[41] H.B. Meyer, Phys. Rev **D76**, 101701 (2007).

[42] E.D. Siggia, B.I. Halperin and P.C. Hohenberg, Phys. Rev. **B13**, 2110 (1975); L.Ts. Adzhemyan, A.N. Vasiliev, Yu.S. Kabrits and M.V. Kompaniets, Theor. and Mathem. Physics **111**, 454 (1999); A. Onuki, Phys. Rev. **E55**, 403 (1997).

[43] S. Jeon, Phys. Rev. **D52**, 3591 (1995).

[44] S. Jeon and L.G. Yaffe, Phys. Rev. **D53**, 5799 (1996).

[45] P. Arnold, C. Dogan and G.D. Moore, Phys. Rev. **D74**, 085021 (2006).

[46] G.D. Moore and O. Saremi, JHEP **0809**, 015 (2008).

[47] L.I.Mandelstam and M.A. Leontovich, ZhETF, **7**, 438 (1937).

[48] L.D. Landau and E.M. Lifshiz, "Fluid Mechanics", Vol. 6, Addison-Westley, 1959.

[49] K. Paech and S. Pratt, Phys. Rev. **C74**, 014901 (2006).

[50] D. Kharzeev and K. Tuchin, JHEP **0809**, 093 (2008).

[51] F. Karsch, D. Kharzeev, and K. Tuchin, Phys. Lett. **B663**, 217 (2008).

[52] H.B. Meyer, Phys. Rev. Lett. **100**, 162001 (2008).

[53] D.N. Voskresensky, Phys. Scripta **47**, 333 (1993).

[54] V.V. Skokov and D.N. Voskresensky, JETP Lett. **90**, 223 (2009); Nucl. Phys. **A828**, 401 (2009).

[55] M. Bluhm, B. Kampfer and G. Soff, Phys. Lett. **B620**, 131 (2005).

[56] Yu.B. Ivanov, V.V. Skokov and V.D. Toneev, Phys. Rev. **D71**, 014005 (2005).

[57] A.S. Khvorostukhin, V.D. Toneev and D.N. Voskresensky, Nucl. Phys. **A791**, 180 (2007).

[58] A.S. Khvorostukhin, V.D. Toneev and D.N. Voskresensky, Nucl. Phys. **A813**, 313 (2008).

[59] C. Sasaki and K. Redlich, Phys. Rev. **C79**, 055207 (2009).

[60] E.E. Kolomeitsev and D.N. Voskresensky, Nucl. Phys. **A759**, 373 (2005).

[61] R. Hagedorn, Supplemento al Nuove Cimento, **III**, 147 (1965); Nuove Cim. **A56**, 1029 (1968).

[62] P. Castorina, J. Cleymans, D. E. Miller and H. Satz, arXiv:0906.2289 [hep-ph].

[63] F. Karsch, arXiv:hep-lat/0601013.

[64] M.Cheng et al., Phys. Rev. **D77**, 014511 (2008).

[65] Christian Schmid, arXiv:0810.0374 [hep-lat].

[66] J. Cleymans, R.V. Gavai and E. Suhonen, Phys. Rep. **130**, 217 (1986).

[67] V.D. Toneev, E.G. Nikonov, B. Friman, W. Nörenbergand and K. Redlich, Eur. Phys. J. **C32**, 399 (2004).

[68] M. Cheng et al., arXiv:0911.2215 [hep-lat]; A. Bazavov et al., Phys. Rev. **D80** 014504 (2009); P. Petreczky (for RBC Collaboration), arXiv:0912.5037 [hep-lat].

[69] Z. Fodor, S.D. Katz and K.K. Szabo, Phys. Lett. **B568**, 73 (2003).

[70] Y. Aoki, Z. Fodor, S.D. Katz and K.K. Szabo, JHEP **0601**, 089 (2006).

[71] J.Theis, G.Graebner, G.Buchwald, J.Maruhn, W.Greiner, H.Stöcker and J.Polonyi, Phys. Rev. **D28** (1983) 2286.

[72] L.P. Csernai and J.I. Kapusta, Phys. Rev. Lett. **69**, 737 (1992); Phys. Rev. **D46**, 4873 (1992).

[73] L.P. Csernai and I.N. Mishustin, Phys. Rev. Lett., **74**, 5005 (1995).

[74] Y. Hama, R.P.G. Andrade, F. Grassi, O. Socolowski Jr., T.Kodama, B. Tavares and S.S. Padula, Nucl. Phys. **A774**, 169 (2006); Y. Hama, R.P.G. Andrade, F. Grassi, O. Socolowski Jr., T.Kodama, B. Tavares and S.S. Padula, AIP Conf. Proc. **828**, 485 (2006) [hep-ph/0510101].

[75] S. Weinberg, *"The quantum theory of fields"*, V.1, Cambridge Univ. press, 1995.

[76] Yu.B. Ivanov, Nucl. Phys. **A474**, 669 (1987).

[77] M.Prakash, M. Prakash, R. Venugopalan and G. Welke, Phys. Rep., **227**, 321 (1993).

[78] E.L. Bratkovskaya and W. Cassing, Nucl. Phys. **A807**, 214 (2008).

[79] M.I. Gorenstein, M. Hauer and O.N. Moroz, Phys. Rev. **C77**, 024911 (2008).

[80] J. Noronha-Hostler, J. Noronha and C. Greiner, Phys. Rev. Lett. **103**, 172302 (2009).

[81] K. Hubner, F. Karsch and C. Pica, Phys. Rev. **D78**, 094501 (2008).

[82] P. Romatschke and T.D. Son, Phys. Rev. D80, 065021 (2009).

[83] J.-W. Chen and J. Wong, Phys. Rev. **C79**, 044913 (2009).

[84] K. Meyer, A. Laesecki and S. Kabelec, J. Chem. Phys. **122**, 012513 (2005).

[85] S. Tomanaga, Z. Phys. **110**, 573 (1938).

[86] J. Cleymans, H. Oeschler and K. Redlich, Phys. Rev. **C73**, 034905 (2006).

[87] A. Andronic, P. Braun-Munzinger and J. Stachel, Nucl. Phys. **772**, 167 (2006).

[88] A.V. Senatorov and D.N. Voskresensky, Phys. Lett. **B219**, 31 (1989).

[89] L.P. Csernai, V.K. Magas, E. Molnar, A. Nyiri and K. Tamosiunas, Eur. Phys. J. **A25**, 65 (2005).

[90] I.C. Arsene, L.V. Bravina, W. Cassing, Yu.B. Ivanov, A. Larionov, J. Randrup, V.N. Russkikh, V.D. Toneev, G. Zeeb, D. Zschiesche, Phys. Rev. **C75**, 034902 (2007); S.V. Akkelin, Y. Hama, Iu.A. Karpenko and Yu.M. Sinyukov, Phys. Rev. **C78**, 034906 (2008).

[91] J. Knoll, Nucl. Phys. **A821**, 235 (2009).

[92] Yu.B. Ivanov, I.N. Mishustin, V.N. Russkikh and L.M. Satarov, Phys. Rev. **C80**, 064904 (2009).

[93] N. Demir and S.A. Bass, Phys. Rev. Lett. **102**, 172302 (2009); Nucl. Phys. **A830**, 733C (2009).

[94] S. Pal, arXiv:1001.1585 [nucl-th].

[95] P. Zhuang, J. Hufner, S.P. Klevansky and L. Neise, Phys. Rev. **D51**, 3728 (1995); P. Rehberg, S.P. Klevansky and J. Hufner, Nucl. Phys. **A608**, 305 (1996).

[96] C. Sasaki and K. Redlich, Nucl. Phys. **A832**, 62 (2010).

[97] R.D. Pisarski, Phys. Rev. Lett. **63**, 1129 (1989); V.C. Lebedev and A.V. Smilga, Ann. Phys. (N.Y.) **202**, 229 (1990).

[98] A. Peshier, Phys. Rev. **D70**, 034016 (2004).

[99] W. Cassing, Nucl. Phys. A795, 70 (2007).

[100] M. Bluhm, B. Kampfer and K. Redlich, Nucl. Phys. **A830**, 737C (2009).

[101] S. Matiello and W. Cassing, arXiv:0911.4647.

[102] S.Gavin and M. Abdel-Aziz, Phys. Rev. Lett. **97**, 162302 (2006).

[103] H.-J. Drescher, A. Dumitru, C. Gombeaud and J.-Y. Ollitrault, Phys. Rev. **C76**, 024905 (2007).

[104] R.A. Lacey, N.N. Ajitanand, J.M. Alexander, P. Chung, W.G. Holzmann, M. Issah, A. Taranenko, P. Danielewicz and H. Stoecker, Phys. Rev. Lett. **98**, 092301 (2007).

[105] A. Adare et al., Phys. Rev. Lett. **98**, 172301 (2007).

[106] A.K. Chaudhuri, Phys. Lett. B681, 418 (2009).

[107] H. Song and U.W. Heinz, arXiv:0812.4274 [nucl-th].

[108] H. Song and U.W. Heinz, Nucl. Phys. **A830**, 467C (2009); A. Monnai and T. Hirano, Phys. Rev. **C80**, 054906 (2009). G.S. Denicol, T. Kodama, T. Koide and Ph. Mota, Nucl. Phys. **A830**, 729C (2009).

[109] P. Bozek, arXiv:0911.2397.

[110] G.S. Denicol, T. Kodama and T. Koide, arXiv: 1002.2394 [nucl-th].

[111] D.N. Voskresensky, Nucl. Phys. **A812**, 158 (2008).

[112] G.M. Bruun and H. Smith, Phys. Rev. **A75**, 043612 (2007).

[113] A. Jakovac, arXiv:0901.2802 [hep-th].

[114] Yu.B. Ivanov, J. Knoll and D.N. Voskresensky, Nucl. Phys. **A672** (2000) 313.

[115] J. Noronha-Hostler, C. Greiner, and I.A. Shovkovyi, Rev. Lett. **100**, 252301 (2008).

[116] A. K. Chaudhuri, arXiv:0910.0979 [nucl-th].

[117] G. Torrieri, B. Tomasik and I. Mishustin, Phys. Rev. **C77**, 034903 (2008); G. Torrieri and I. Mishustin, Phys. Rev. **C78**, 021901(R) (2008); R.J. Fries, B. Muller and A. Schafer, Phys. Rev. **C78**, 034913 (2008).

[118] Ya.B. Zeldovich and A.S. Mikhailov, UFN (Sov.) **187**, 467 (1987).

[119] R. Rapp and H. van Hees, Braz. J. Phys. **37**, 779 (2007).